



SESAME

Research and Innovation Action (RIA)

This project has received funding from the Euratom research and training programme 2014-2018 under grant agreement No 654935.

Start date : 2015-04-01 Duration : 48 Months
<http://sesame-h2020.eu/>



Meliloo: pre-test simulations and measurements

Authors : Tomas MELICHAR, Miloslav BELKA, Otakar FRYBORT, Michal KORDAC
with contribution from CRS4: Manuela Profir and Vincent Moreau

SESAME - Contract Number: 654935
thermal hydraulics Simulations and Experiments for the Safety Assessment of Metal cooled reactors

Document title	Meliloo: pre-test simulations and measurements
Number of pages	45
Author(s)	Tomas MELICHAR, Miloslav BELKA, Otakar FRYBORT, Michal KORDAC with contribution from CRS4: Manuela Profir and Vincent Moreau
Document type	Deliverable
Work Package	WP3
Issued by	CVR
Document number	D3.10
Date of completion	2018-07-16 09:31:23
Dissemination level	Public

Summary

In the first part of this report, a computational CFD model which was developed for simulations of liquid metal natural convection and freezing is described along with the first results. The model will be validated on the experimental data obtained from the experimental stand for investigation of lead freezing. This stand was designed, constructed and commissioned at Research centre Rez and is described in the second part of this report. After that, data obtained during the first experimental run can be found. In the appendix of this report, a CFD model developed at CRS4 is described and first results are presented.

Approval

Date	By
2018-07-16 13:23:19	Mrs. Vincent MOREAU (CRS4)
2018-07-16 23:30:50	Dr. Mariano TARANTINO (ENEA)

Table of contents

1 Introduction4

2 Development of computational model and pre-test simulations4

 2.1 Modelling strategy..... 4

 2.2 Computational model..... 5

 2.2.1 Geometry..... 5

 2.2.2 Mesh..... 6

 2.2.3 Solver settings 7

 2.3 Results 8

 2.3.1 Steady-state 8

 2.3.2 Transient..... 9

 2.3.3 Conclusion of the pre-test simulations 11

3 Experimental campaign 11

 3.1 Description of the facility 12

 3.1.1 The primary system 12

 3.1.2 The secondary system 17

 3.1.3 The auxiliary system..... 17

 3.2 Commissioning 18

 3.3 The experimental data 21

4 Conclusions..... 27

5 Reference..... 28

6 Appendix – CFD model of CRS4 29

Abbreviations

<i>BC</i>	<i>Boundary Condition</i>
<i>CFD</i>	<i>Computational Fluid Dynamics</i>
<i>CRS4</i>	<i>Center for Advanced Studies, Research and Development in Sardinia</i>
<i>CVR</i>	<i>Research centre Rez</i>
<i>DAQ</i>	<i>Data Acquisition System</i>
<i>EV</i>	<i>Experimental Vessel</i>
<i>HLM</i>	<i>Heavy Liquid Metal</i>
<i>HTC</i>	<i>Heat Transfer Coefficient</i>
<i>MFR</i>	<i>Mass-Flow Rate</i>
<i>RANS</i>	<i>Reynolds-Average Navier-Stokes</i>
<i>SV</i>	<i>Storage vessel</i>
<i>TC</i>	<i>Thermocouple</i>
<i>UDF</i>	<i>User Defined Function</i>

1 Introduction

An activity focused on development and validation of computational tools for modelling of solidification phenomena, which is essential for safety analyses of the heavy liquid metal (HLM) cooled reactors, is ongoing within H2020 SESAME project WP3. A particular task of this activity, which is ongoing at Research centre Rez (CVR), deals with the production of an experimental dataset on lead freezing for the codes validation as well as with the development of a CFD model able to solve the related physical phenomena. This deliverable describes in details the CFD model developed using the ANSYS FLUENT 17 code along with the first experimental results. Selected modelling strategy, computational geometry and mesh, solver settings and the model testing are contained in section 2. In parallel, another CFD model was developed at CRS4; the description of this model is also included in appendix. Section 3 is focused on the experimental facility fabrication and commissioning phase. The facility allows to investigate experimentally the natural convection of liquid lead in a pool-type geometry and to study its freezing under different operational conditions. The final design of the facility is given in section 3. The main challenges, which were faced during the commissioning phase, are also reported. The first measured data for the stand verification are presented in section 4. The work described here follows the previous deliverable describing in details the design of the mechanical part of the facility and of the control and data acquisition (DAQ) system [1].

2 Development of the computational model and pre-test simulations

This section is focused on the CFD tool intended for modelling of both natural convection and freezing of liquid metal developed at CVR. The model is based on the proposed design of the experimental stand (described in details in section 3). Preparation and preliminary testing of the model along with the first results will be described in this section.

2.1 Modelling strategy

During the first stage, various modelling strategies were considered in order to select the most appropriate approach for this application. While the HLM in the main experimental vessel (EV) is required to be modelled using CFD, the air cooling system of the facility, intended for the heat removal from the EV, is not the main object of interest and its modelling might therefore be simplified. Moreover, due to very different properties and physical phenomena solved in the two fluid domains, issues with the implementation of both fluids into a single computational model can be expected.

For this reason, three modelling strategies (shown in Figure 2-1) were proposed and investigated; (1) coupling of 1D and CFD model, (2) coupling of two CFD models and (3) implementation of both fluids into a unique common CFD model.

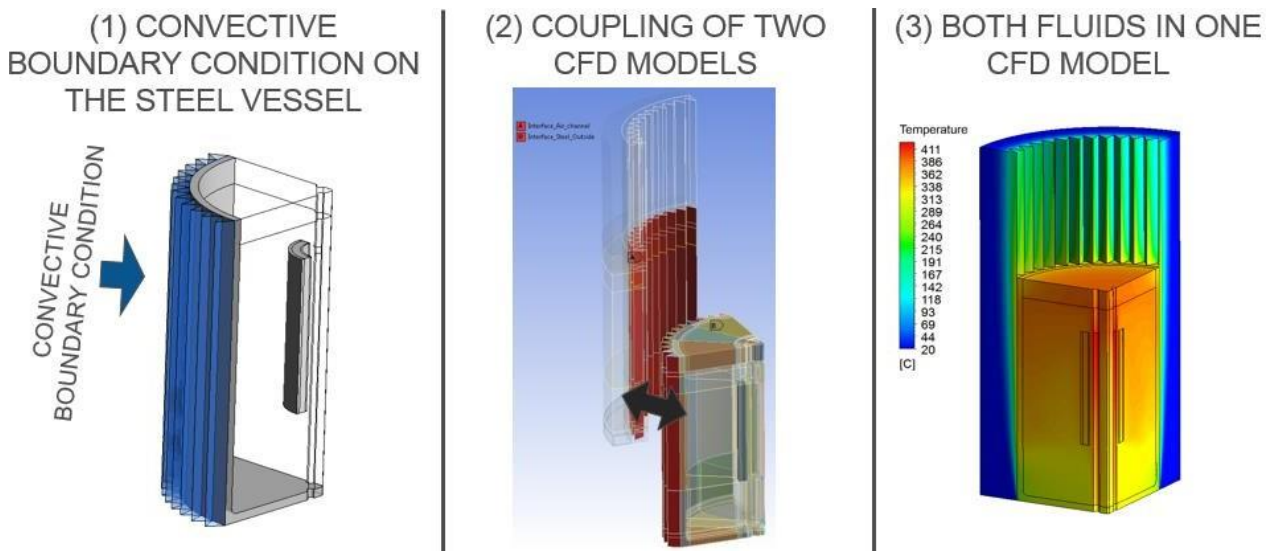


Figure 2-1: Modelling strategies

The first approach (Figure 2-1 - left) is based on the application of a convective boundary condition on the external surface of the EV, which is facing the cooling air. The heat transfer coefficient (HTC) of the air can be obtained from an appropriate correlation and the air bulk temperature can be determined using the energy balance equation. This approach is the most appropriate in terms of computational time, however its accuracy has been considered unacceptable. The temperature field in the lead is very sensitive on the air cooling and no correlation can ensure a sufficient accuracy of the HTC for the air channel geometry. Moreover, the likely non-uniformity of the convective heat transfer on the ribbed surface cannot be predicted.

The second approach (Figure 2-1 - middle) deals with the possibility of coupling two separate CFD models, thus allowing a different solver settings for each fluid domain. This approach requires data transfer between the models and therefore the preparation of a user defined interface; the most appropriate way seems to be transferring the heat flux on the external surface of the EV. The interface was prepared using user defined functions (UDF) and programming language SCHEME [2], both are implemented in ANSYS FLUENT 17.0. This option was found able to deal with the two fluids, however the computational time increased significantly due to the data transfer. Therefore, this approach was considered unsuitable for the transient analyses. Another limitation is the need to use two solver licenses.

The last proposed option (Figure 2-1 - right) is based on the implementation of both fluids into one single CFD model. This approach was selected because expected to give a sufficient accuracy together with an acceptable computational time. However, it is impossible to use different turbulence models within the same CFD model. Therefore, it was necessary to tune the computational mesh and the solver setting in order to capture all the physical phenomena occurring in the fluids and in order to obtain stable and convergent solutions. The appropriate solver setting is described and justified in section 2.2.3.

2.2 Computational model

The CFD model was prepared using the ANSYS software; particular parts are explained in this section. The following features are required from the computational model:

- Solution of the heat transfer, natural convection and freezing in the lead volume
- Solution of the heat conduction in the EV and the heaters
- Accurate modelling of the heat removal system
- Ability to solve both the steady-state and transient cases
- Sufficient accuracy and reasonable computational time.

The CFD model has to be able to deal with these features, which must therefore be considered within all phases of preparation of the model.

2.2.1 Geometry

The computational geometry was prepared using the *ANSYS DesignModeler* tool and is based on the design of the experimental facility, however some simplifications were adopted. One quarter of the EV is modelled due to symmetry. Individual geometrical parts of the model and their main characteristics are described below; the geometrical model is schematically shown in Figure 2-2 left. In Figure 2-2 right, the computational model created using DesignModeler is depicted. Partition of the model into smaller volumes is desirable for meshing reasons; the structured hexahedral mesh can then more easily be defined in the particular volumes which are described hereafter

- **Fluid domain – Lead.** Closed volume of the liquid (or partially liquid) metal where the natural convection and freezing of the lead is solved.
- **Solid domain – Experimental vessel.** Steel solid domain representing the EV. The EV is equipped with triangular ribs on the external surface to increase the heat transfer area. A 3° chamfering at the bottom of the EV intended to facilitate draining is neglected in the model as well as the extension of the EV diameter at the flange connection at the top part of the EV.
- **Solid domain – Heaters.** Four cylindrical electric heaters with heating power of 2 kW each are placed in the centre of the EV. The heaters are basically composed of three parts and different materials which allow to accurately simulate a detailed temperature field.
- **Solid domain – Obstacle.** An internal obstacle is intended to streamline the natural circulating liquid metal (the lead will flow around the obstacle). In the first model the obstacle has a cylindrical shape,

but different shapes will be used in the future experimental campaign. Two screws that connect the obstacle to a lid of the EV are neglected.

- **Solid domain – Argon layer.** In the experiment, the function of an argon layer over the lead volume is to accommodate for the lead volumetric expansion and to ensure a slight over-pressure, thus avoiding air penetration into the EV. Although the argon layer is a fluid, its modelling as a solid part is acceptable since the effect of convection is not expected to be significant. The thermal expansion of the lead is not considered in this model (Boussinesq approximation).
- **Fluid domain – Air.** The second fluid domain represented the air coolant. The air is forced by a radial fan providing mass-flow rate (MFR) in range between 0–0.2 kg/s in the experimental facility. Only the part of the air channel adjacent to the EV is considered. Straight extension below and above the vessel were added to ensure a developed turbulent flow and to avoid back-flow effects at the outlet. The MFR in the air channel is defined using “velocity inlet” boundary condition located at the bottom part of the domain.

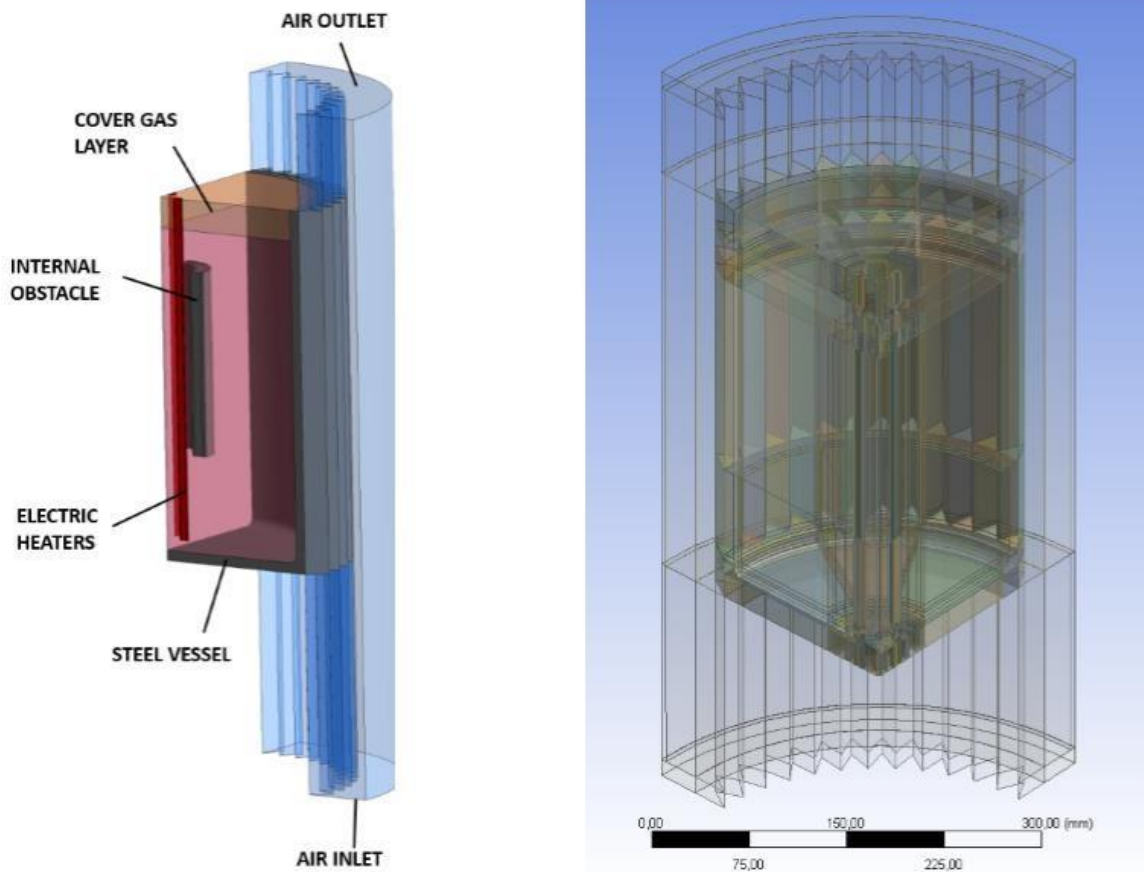


Figure 2-2: Computational geometry

2.2.2 Mesh

Different computational meshes have been tested before a stable and mesh-independent solution was reached. At the end, a hexahedral, partially structured/unstructured mesh was selected. The main findings and recommendations obtained from the mesh studies are following:

- The hexahedral mesh is compatible with ANSYS FLUENT and gives the best ratio between mesh size and accuracy. The polyhedral mesh was tested unsuccessfully.
- A structured mesh was prepared in the lead domain; a partially structured mesh (due to geometric complexity) is built in the steel vessel and the air channel. A structured mesh in the boundary layer of the air channel is strongly recommended.
- Conformal mesh between the lead and the heaters is necessary to avoid solver failure.
- A non-conformal interface between the air and the vessel is acceptable.

- A fine mesh is required close to the heaters and at the bottom part of the obstacle. This is required especially during transient simulations when the solid front reaches the obstacle and the flow area is limited.

Mesh sensitivity of both fluid domains on the lead parameters was studied. The results are shown in Table 1. It is obvious that the observed lead parameters are not very sensitive on the mesh size of the lead domain. However, the mesh size of the air channel affects the results significantly. The lead temperature field is very sensitive on the air cooling modelling, a point which should be taken into consideration.

Table 1: Mesh sensitivity study

Air channel mesh elements no.	Lead mesh elements no.	Heat transfer coefficient in the air channel	Max. velocity in lead	Max. lead temperature
1.17 M	1.8 M	11.95 W/m ² k	0.0394 m/s	675.4 K
2.17 M	1.8 M	11.74 W/m ² k	0.0392 m/s	681.3 K
4.34 M	1.8 M	11.63 W/m ² k	0.0391 m/s	684.5 K
2.17 M	1 M	11.74 W/m ² k	0.0392 m/s	681 K
2.17 M	3.7 M	11.74 W/m ² k	0.0393 m/s	681.5 K

Based on the above mentioned findings, a mesh composed of approx. 4.5 M elements (1.8 M in the lead, 2.17 in the air channel and 0.5 M in the solid bodies) was selected. The mesh is shown in Figure 2-3. Quality parameters of the selected mesh are shown in Table 2.

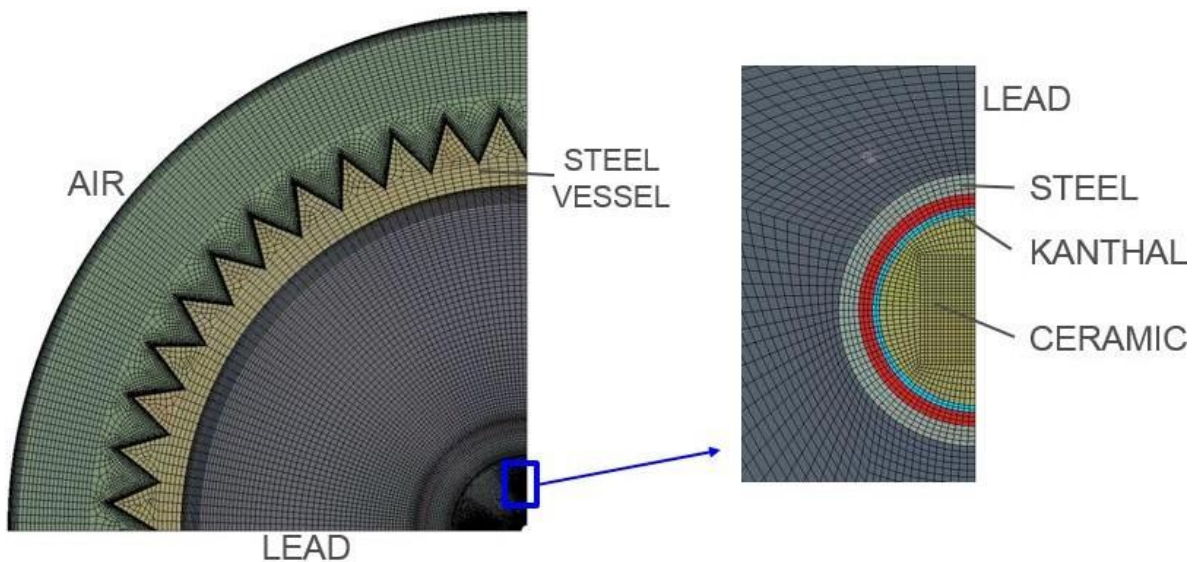


Figure 2-3: Computational mesh

Table 2: Mesh quality parameters

Max/Average Aspect Ratio	61/5.7
Min/Average Orthogonal quality	0.45/0.87
Max y+	4.99

2.2.3 Solver settings

Like the mesh, different settings of the numerical solver and of the turbulence model were tested in order to obtain a suitable configuration leading to a convergent and stable solution. RANS models were considered as a reasonable option for this application in terms of accuracy and HW costs. Due to the presence of the two fluids, the k-epsilon RNG [3] turbulence model was selected. The turbulent Prandtl number is resolved numerically (unlike other RANS models where it is assumed constant) in this model which allows to handle the differences in convective heat transfer between the lead and air domains. The turbulent Prandtl number is

expected to be significantly lower for HLM than for the air [4]. The option of “enhanced wall treatment” was used to avoid wall functions in the boundary layer. The *SIMPLE* scheme was used for pressure-velocity coupling, discretization schemes of *second order* or *second order upwind* were used for pressure, momentum, k and epsilon. The unsteady calculations can be run with relatively high time steps (1 s), which compensates for the large mesh in terms of computational time. However, the time steps should be decreased at some parts of the simulation (especially when the frozen front is reaching the obstacle and the number of mesh elements on the flow area is low) to avoid solver failures. Tuning of under-relaxation factors at this phase and also at the beginning of the freezing was also necessary.

As shown in Figure 2-2, inlet boundary condition (BC) is applied on the bottom face of the air channel and is represented by inlet velocity corresponding to the current MFR and by inlet air temperature (20°C assumed). The pressure outlet BC is set at the top face. Other external walls of the EV which are not cooled by air as well as the external surface of the air channel are set as adiabatic. The heating is set as a volumetric source corresponding to the current heating power in the kanthal part of the heaters.

The physical properties of the lead were taken from [5] and implemented into the solver in the form of piecewise linear functions with respect to temperature. Air and argon properties were taken from [6]. Stainless steel 321 was used as the EV material and the properties were taken from [7]. Properties of the Kanthal which is used as a heating element in the heater can be found in [8].

An existing FLUENT’s module “Solidification” was used for the freezing simulations. The Module is based on an enthalpy-porosity technique. A quantity called the liquid fraction indicated fraction of the cell volume that is in liquid form based on the enthalpy balance. Setting of zero porosity to the cells where the material is fully solidified is being applied [3]. Additional physical properties required by the module are the melting point (600.6 K) and the latent heat of melting (23 070 J/kg).

2.3 Numerical results

Both steady and transient pre-test simulations were performed. The main purpose of the pre-test simulations is to test the developed CFD model and to provide more in-depth insight into the temperature distribution in the EV and into the operational parameters. The data obtained from these simulations have been utilized for the commissioning of the experimental stand.

2.3.1 Steady-state

At the first stage, operational parameters representing potentially interesting states were subject of investigation. These states include the state where all the lead is melted and at a slightly higher temperature than melting temperature (327.5 C) and the states where a specific fraction of the lead is solidified. The parameter values has been obtained iteratively using steady-state simulations with constant air mass-flow rate and heating power. Based on the simulations, the parameters leading to different solid fractions are listed in Table 3. In all cases, the total heating power was fixed to 3 kW; for air flow rates lower than 0.145 kg/s, the lead remains fully liquid. The state when the solid front is reaching the obstacle was obtained for MFR of 0.176 kg/s. It has been clearly established that a relatively low change of the air mass flow rate causes a significant difference in the lead temperature and frozen volume.

Table 3: Results of steady-state simulations

Case	Air MFR [kg/s]	Heaters power [kW]	Solid fraction [%]	Max lead temp. [°C]	Min lead temp. [°C]	Max lead velocity [m/s]
1	0.145	3	0	422.2	333.3	0.0373
2	0.152	3	3	407.8	318.6	0.0375
3	0.160	3	15	394.0	304.5	0.0391
4	0.176	3	42	378.2	274.0	0.0394

The main variables are depicted in Figure 2-4. Temperature field in the EV for cases 2 (left), 3 (middle) and 4 (right) of table Table 3 are shown in Figure 2-4 top. In Figure 2-4 bottom, contours of velocity are depicted along with the frozen structure shape.

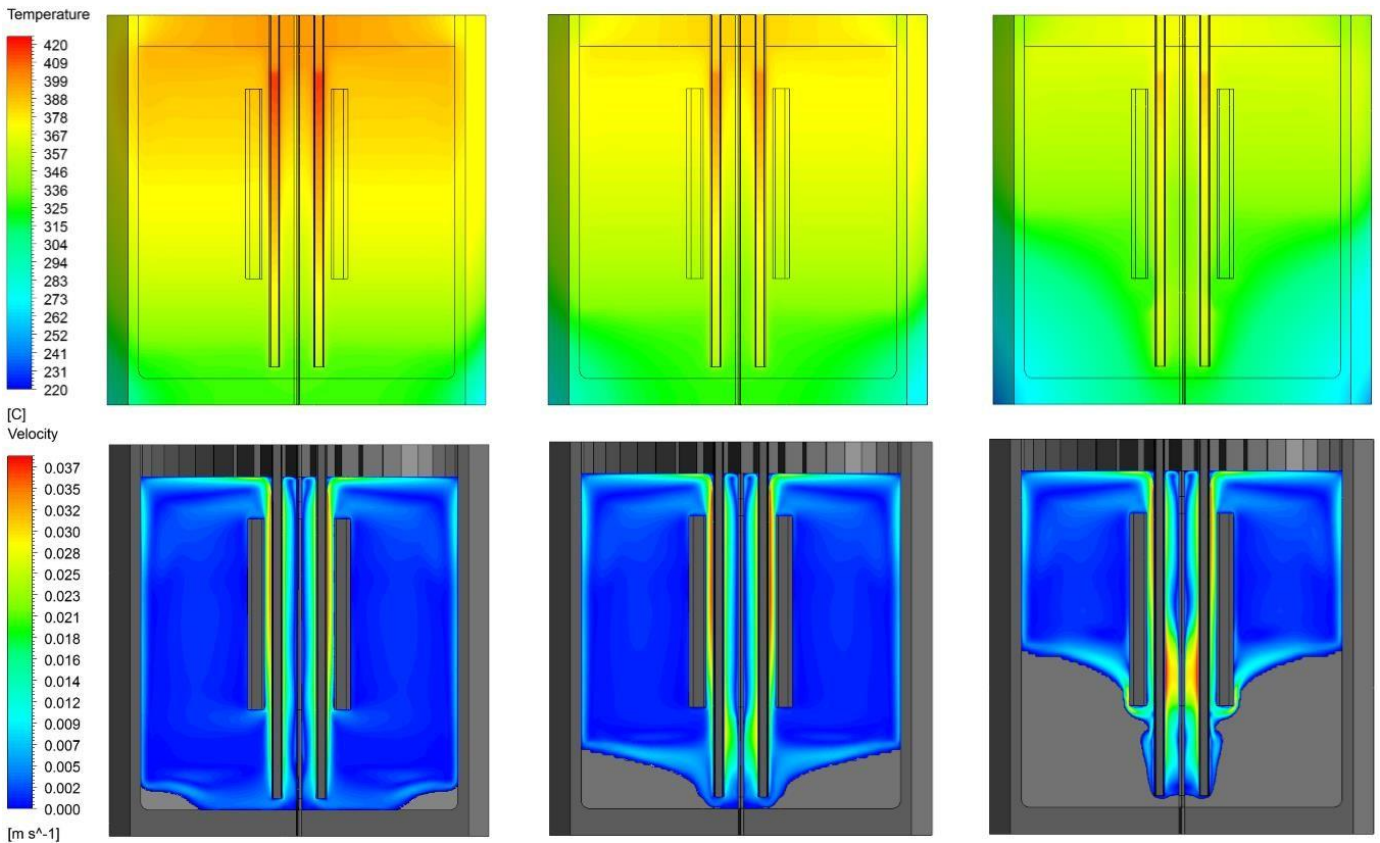


Figure 2-4: Temperature and velocity field for steady-state calculations, in particular case 2 (left), case 3 (middle) and case 4 (right)

2.3.2 Transient

The pre-test transient simulations are needed to evaluate the freezing speed in the EV. For this purpose, the steady-state results corresponding to the fully liquid state (case 1 in Table 3) were used as initial conditions and then the air MFR was increased to the maximum value (0.5 kg/s). The evolution of the temperature field and the frozen front development is shown for selected times in Figure 2-5. It can be seen that the freezing process is relatively long – approx. 70% of the lead is in solid state after 40 minutes of transient. The 3D shape of the frozen structure is depicted at three different times in Figure 2-6 using the SW ANSYS CFD Post tool. This kind of output will be used for comparison with experimental data; the liquid content of the partially frozen EV will be drained at a given time and the shape of the frozen part remained in the EV can be extracted and converted in numerical data using a 3D scanning.

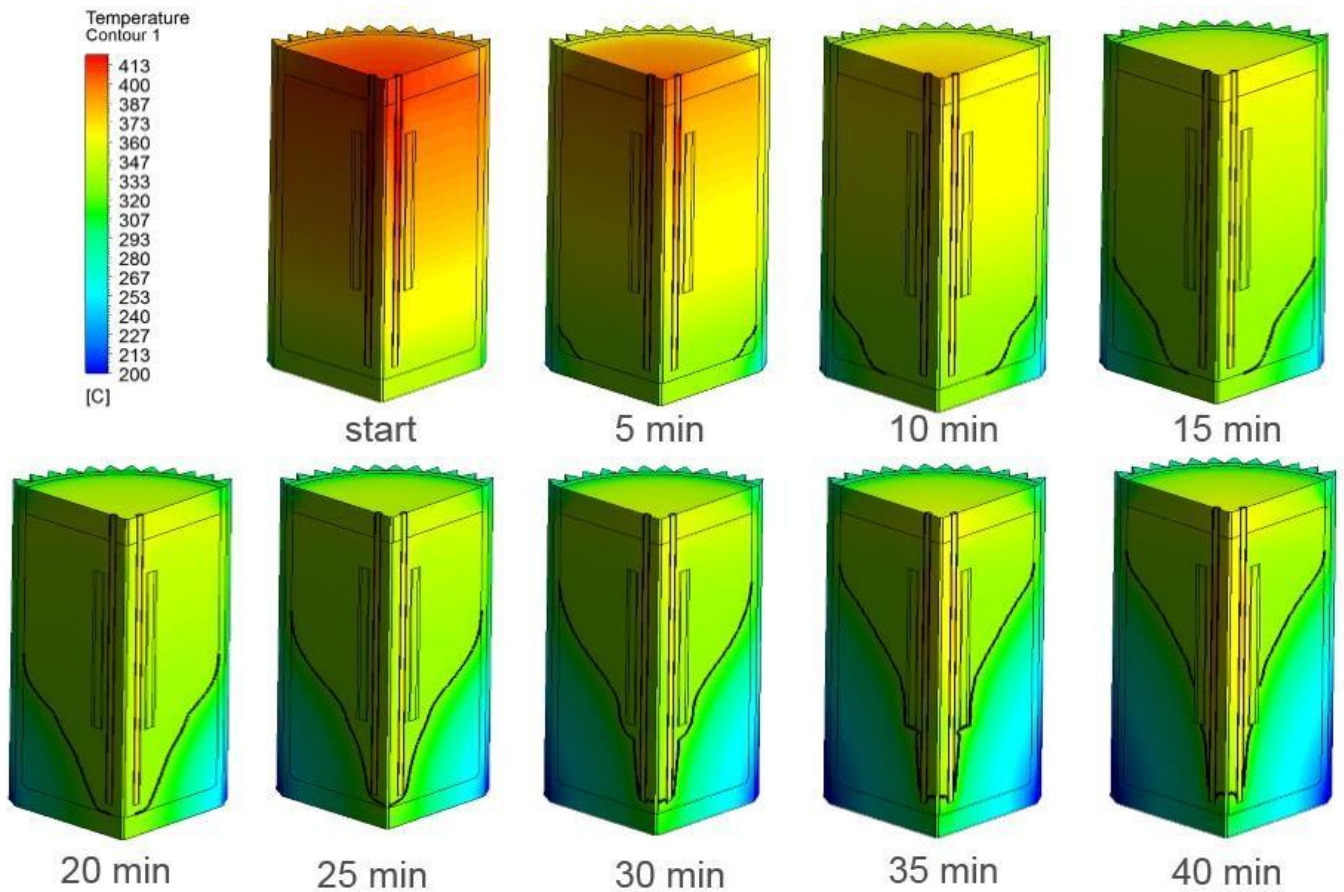


Figure 2-5: Temperature field at different times of transient simulation

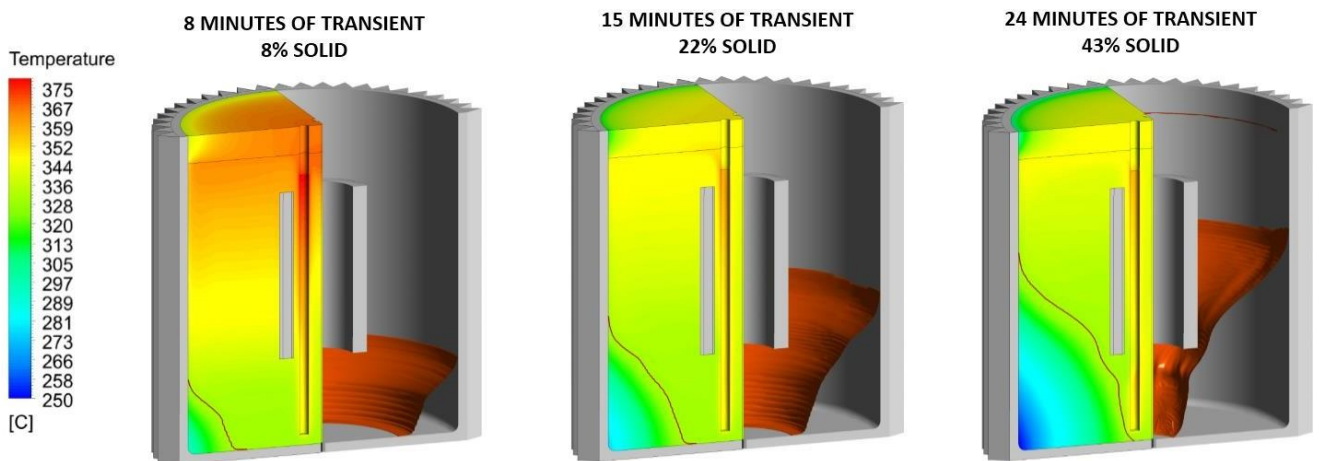


Figure 2-6: 3D shape of the frozen structure from the model

Another important output of the transient simulation is development of temperature of the main heaters, which is shown in Figure 2-7. Increase of the maximum temperature of the heaters which appears approx. after 30 min of the simulation is caused by suppression of natural convection when the frozen front reaches the obstacle and therefore cooling of the heaters is reduced. The results proved that the model is capable to predict this phenomena which can be also benchmarked through thermocouples located inside the electric heaters.

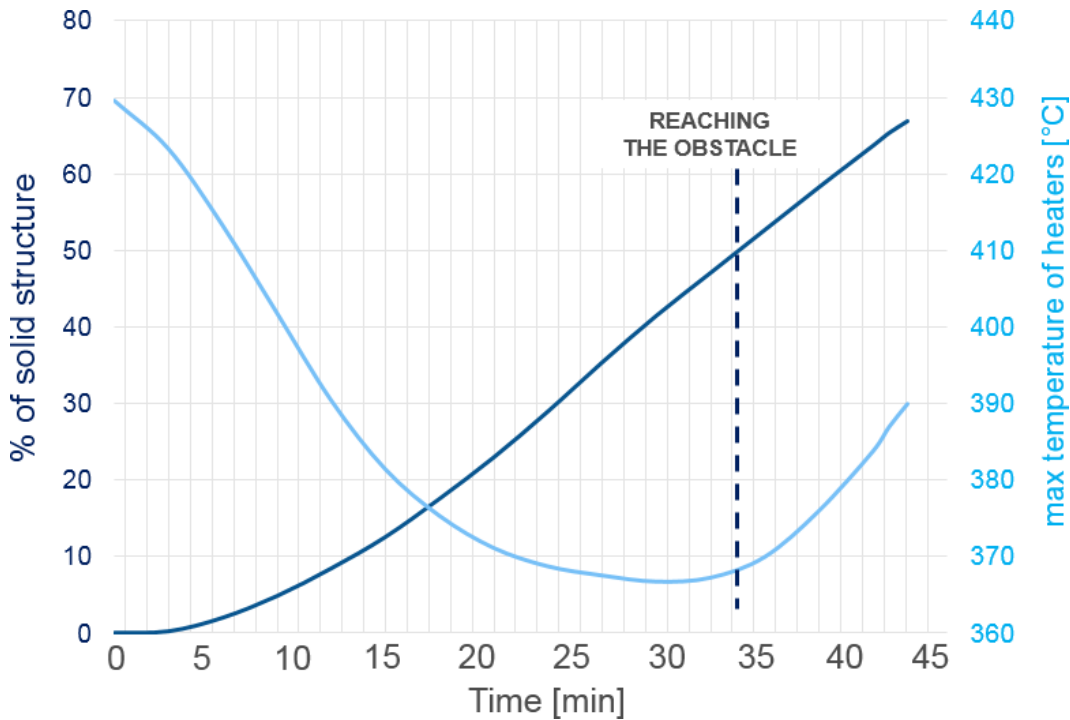


Figure 2-7: Transient results of the heaters temperature

2.3.3 Conclusion of the pre-test simulations

A CFD model for the simulation of liquid metal flows and freezing was developed and is capable to perform both steady-state and transient simulations. The main findings from the development phase of the CFD model are following:

- High quality structured and conformal mesh is needed to avoid the solver failures during the calculations.
- K-epsilon RNG model of turbulence can be a good choice for model with different fluids since the turbulent Prandtl number is being resolved numerically.
- Extensive tuning of the solver settings (relaxation factors and time steps) is needed during the freezing process, especially when the frozen front is reaching the obstacle.
- The air cooling has to be modelled with high precision because of its high influence on the lead temperature field. Particular attention has to be focused also on the air channel during collection of the experimental data to evaluate the accuracy of the air cooling modelling.

The results of the model provide support for the commissioning of the experimental stand. Setting of the heaters power and air mass-flow rate at the experimental stand will be based on the results obtained from the steady-state simulations. In the following stage, another simulation for various conditions representing the stand operation will be carried out and the model will be validated on the measured experimental data. Moreover, another CFD model is being developed independently by the project partner CRS4 using the commercial CFD code STAR-CCM+ (see section 7 - Appendix) so the results will be compared also with the model created in a different way and the differences between the model will be evaluated.

3 Experimental campaign

For the proper development and validation of the simulation tools, experimental data are essential. At the Research Centre Rez, Meliloo loop was operated to study the thermal-hydraulics and corrosion processes of the Pb-Li eutectics. The original proposal dealt with intention of modifying the loop in order to produce freezing experiments. However, due to complexity of the reconstruction and unsuitability of operational parameters of the Meliloo loop, a new stand-alone experimental stand for freezing experiments, working with naturally circulating lead, was proposed and built at CVR. The modified SESAME experimental facility was designed for

testing, controlling and elucidation of the solidification processes under different conditions. The operating conditions were set by controlled electric heating and air cooling of the experimental vessel.

This report describes the entire SESAME facility in details. The first part includes the design and manufacture of the components. The second part covers a commissioning of the experimental setup. The third part consists of the initial experimental data. The last chapter delineates the future experimental plan.

3.1 Description of the facility

The sketch of the SESAME facility is depicted in Figure 3-1. It consists of three main systems: primary, secondary, and auxiliary. The primary system is the section that contains the pure lead. It is composed of the EV, a draining pipe, and a storage vessel (SV). The secondary system represents the cooling system that includes an air fan, an air duct around the experimental vessel, and a section for airflow rate measurement. The auxiliary system serves as gas and water supply.

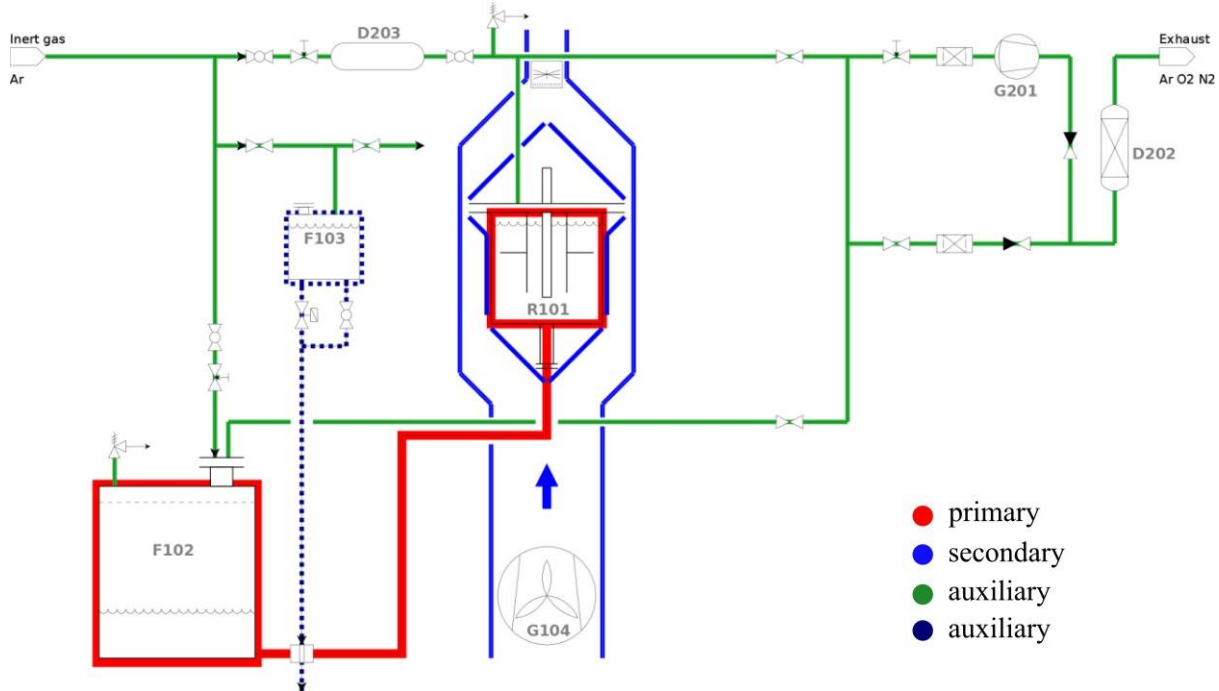


Figure 3-1: The experimental facility design with the arrangement of the main systems

3.1.1 The primary system

The pure lead circulates in the primary system. This system consists of the EV, the draining pipe, and the SV. During operation, the liquid lead is first pushed from the SV through the draining pipe to the EV. After that, the draining pipe is clogged to prevent lead backflow. The EV is heated by heating rods and cooled by air flowing around. This configuration with external air cooling and internal heating allows to generate a natural convection pattern. By adjusting the parameters, the lead temperature decreases and a subsequent solidification can occur.

The EV (Figure 3-2) is a cylindrical pool of internal diameter and height of about 30 cm. It was manufactured by casting method (COMTES FHT, Dobruška, Czech Republic) and the material used was stainless steel. The surface finishing of the EV interior was done at Balasi s.r.o. (Celakovice, Czech Republic) to achieve a suitable roughness and precise dimensions. The exterior surface is covered by fins to increase heat transfer. The EV interior contains heaters and various instruments to study the solidification process, such as thermocouple (TC) probes, simple TC, laser level measurement instruments, and inner obstacles.

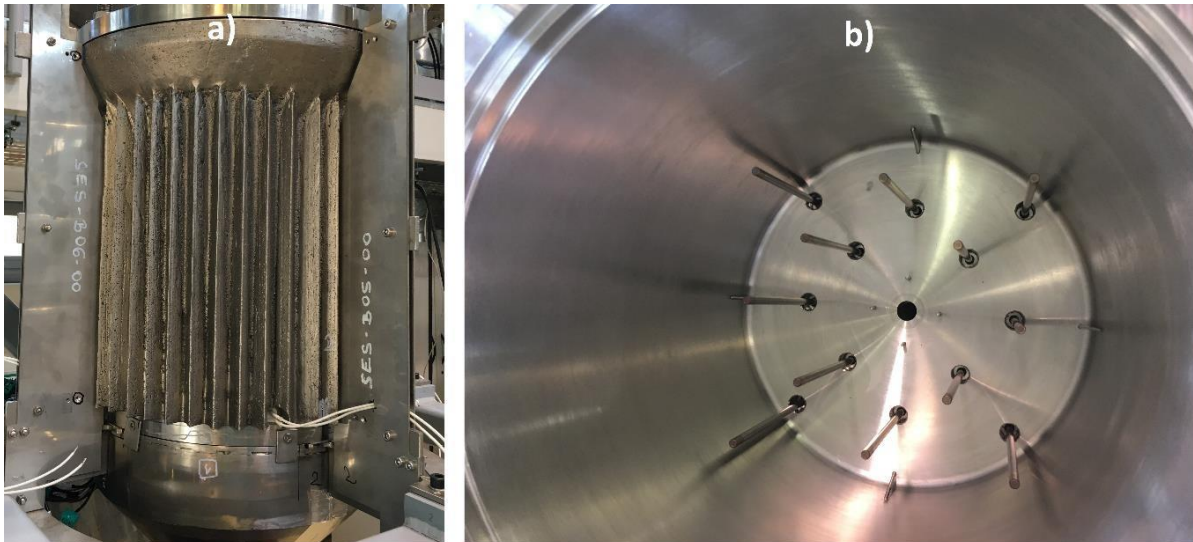


Figure 3-2: The external (a) and internal (b) view of the experimental vessel

To acquire spatial temperature information, multilevel TC probes were developed at Sensit s.r.o. (Roznov pod Radhostem, Czech Republic). Each probe contains several (five or nine) K-Type TCs having diameter of 1 mm. The probes were manufactured as hollow tubes (outer diameter of 6 mm). The TCs were placed inside and the residual space was filled with MgO powder. The end of each probe was sealed with a duralumin piece, which was pressed against the probe wall to ascertain a fixed position of all the TCs. The TC probes allow temperature measurement up to 600 °C. There are 21 TC probes in total. Twelve probes are attached to the EV bottom using a demountable fitting (Swagelok, OH, USA) (Figure 3-2b). Nine probes are connected to the EV lid via a demountable fitting (Swagelok, OH, USA) (Figure 3-3).

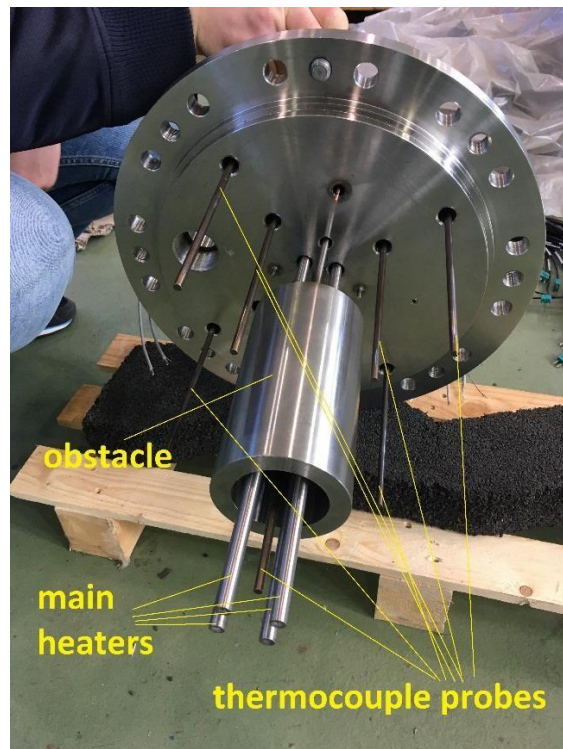


Figure 3-3: The lid of the experimental vessel with various instrumentation

The numbering of the TC probes can be seen in Figure 3-4. The probes numbered from 1 to 12 are attached to the EV bottom. The probes 13 to 21 are attached to the EV lid. Each probe except the probe 21 contains five TC sensors. The distance between TCs in a probe is 30 mm and the first TC in each probe is located 3 mm from the probe tip. Every TC sensor has its own number to properly determine its location. The TC sensor

number contains the probe number and then its position in the probe. The sensor at the probe tip has number 01 while the sensor farthest from the tip has number 05. Therefore, the TC at the tip of the probe 14 has a number T1401 and the TC farthest from the probe tip has a number T1405 (Figure 3-4).

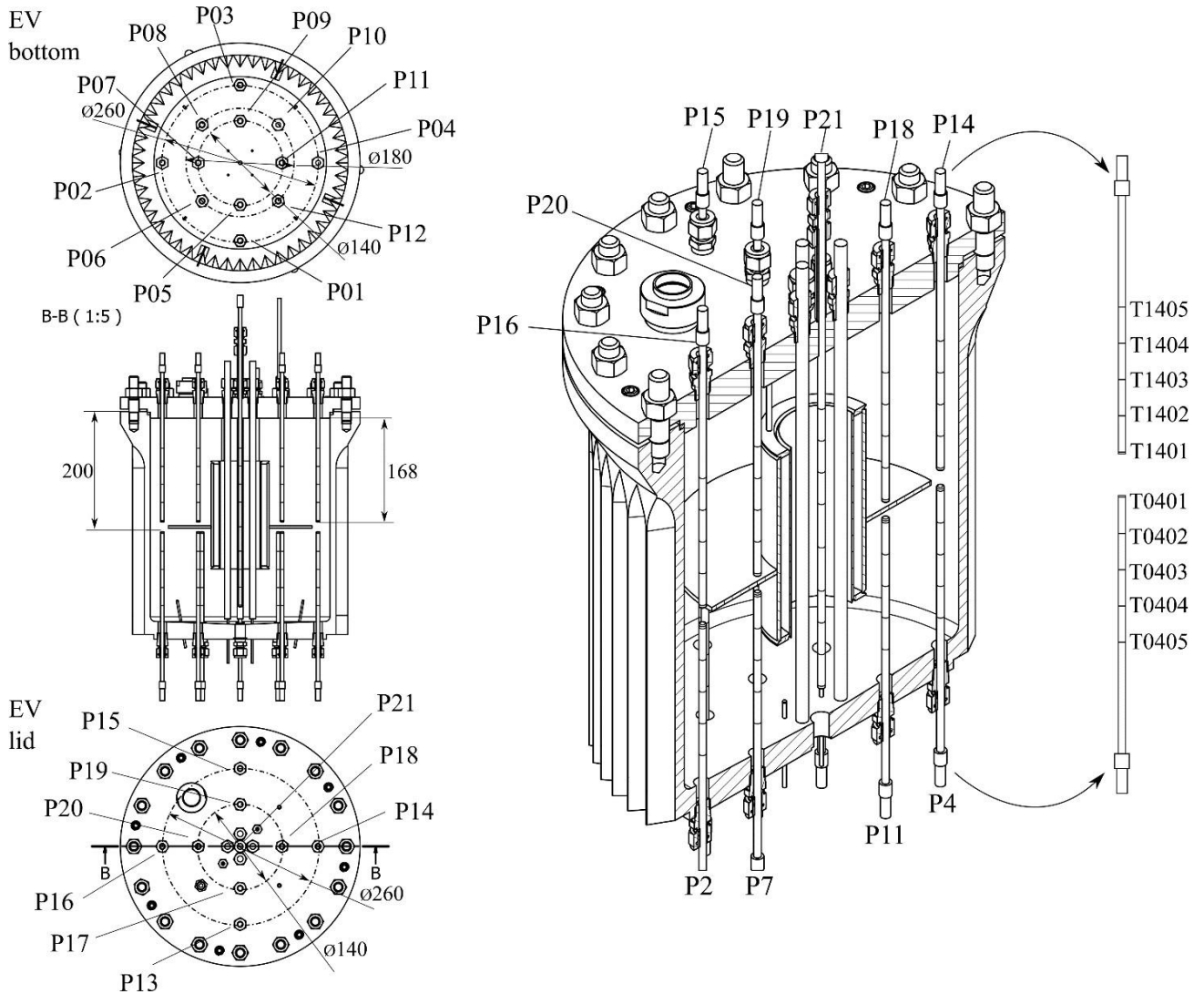


Figure 3-4 Numbering and locations of the probes and thermocouples

There are eight other simple TC sensors in the EV bottom having diameter of 1 mm. They are placed inside TC wells (Figure 3-5). The location of the TC wells are in the areas of the lowest expected temperature, i.e. the areas of initial solidification. All the data from the probes and simple TC are acquired via DAQ module (National instruments Corporation, Texas, USA).

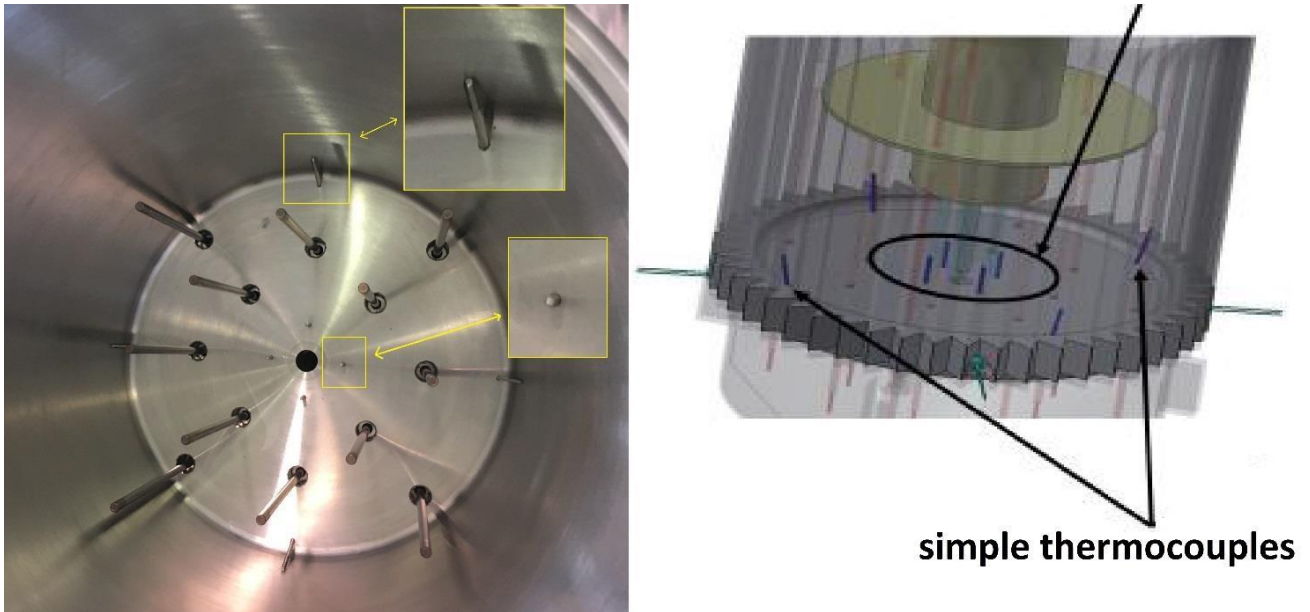


Figure 3-5: Thermocouple wells for simple thermocouple sensors and their layout

Lead level information is obtained by either a contact or a laser sensor. The contact sensor is a CeramTec feedthrough 3887-12-W (Ceramtec, Plochingen, Germany). This feedthrough is actually a conductor that transfers electrical power while in contact with liquid lead (Figure 3-6). This sensor is employed mainly during the EV filling and is placed in the EV lid. The other sensor is a CMOS laser sensor Omron ZX1 (Omron, Tokyo, Japan). This sensor is used for continuous lead level measurement. The laser beam goes in and out of the experimental vessel through a sight glass in the lid. As the sensor can be used only in room conditions, a distance tube was designed to provide thermal insulation (Figure 3-6).



Figure 3-6: Lead level sensors; laser level measurement (left), contact level sensor (right)

The design of the experimental setup is such that a natural circulation pattern occurs in the EV. To investigate this phenomenon, two types of inner obstacles were designed and manufactured (Figure 3-3 and 3-7). The obstacle for the initial measurements has a cylindrical shape with outer diameter of 100 mm, inner diameter of 70 mm and height of 180 mm. The second obstacle has a ring welded to its external wall in order to decrease

a space between the obstacle and the EV wall. The ring outer diameter is 240 mm. Each obstacle is attached to the EV lid via a steel tubing and a demountable fitting in order to provide exchangeability.



Figure 3-7: An inner obstacle with a ring

The heating in the EV is provided by main and auxiliary heating rods (Eltop s.r.o., Miretice, Czech republic). The four main heating rods with controlled heating power are attached to the EV lid. The maximum heating power of each rod is 2 kW. The heated part of the rod has a length of 280 mm and the rod diameter is about 10 mm. A TC is included inside each heating rod to prevent overheating. The auxiliary heaters (Figure 3-8) are placed inside the EV bottom to prevent lead solidification during experimental vessel filling. There are four auxiliary heaters, each of which has a 500 W heating power. The auxiliary heaters have a diameter of 8 mm and a length of 130 mm.



Figure 3-8: Auxiliary heating rods

The SV is a cylindrical pool with internal diameter of 315 mm and height of 625 mm. Its function is to storage lead when the experimental setup is not in operation. In order to liquefy the lead before filling up the EV, the SV is equipped with three ceramic band heaters (Acim Jouanin, Cedex, France). Each heater has a maximum

heating power of 2kW. There are two simple TC sensors to monitor temperature in the SV. The lid of the SV has a sight glass to check the lead level via CMOS laser sensor Omron ZX1 (Omron, Tokyo, Japan).

The SV is connected to the EV by a draining pipe. There are several simple TC sensors to monitor the lead temperature and to prevent pipe plugging before the filling up is completed. The pipe is heated by both heating cables and tapes. Each heater is controlled separately. The heaters are insulated together with the pipe by a few centimeter-thick glass wool insulation.

3.1.2 The secondary system

The function of the secondary system is to provide controlled cooling of the EV. This system consists of an air fan, an air channel, and sensors for measuring flow rate and temperature (figure 3-9). The air channel around the EV is demountable to provide access to handling with the vessel. The channel is divided into four axisymmetric sections around the EV, each of which could be sealed resulting in asymmetric cooling.

The required MFR through the air channel is supplied by a circular duct fan KD 355E (Systemair AB, Skinnskatteberg, Sweden). The fan is placed under the EV. The rotation speed is controlled by a frequency converter. The MFR through the air channel is measured via a Wilson flow Grid and a pressure difference converter (Airflow Lufttechnik GmbH, Rheinbach, Germany). The Wilson flow grid works on the principle of measuring a difference in total and static pressure. Two resistance thermometers were placed downstream and upstream of the experimental vessel to monitor the temperature difference and heat transfer.

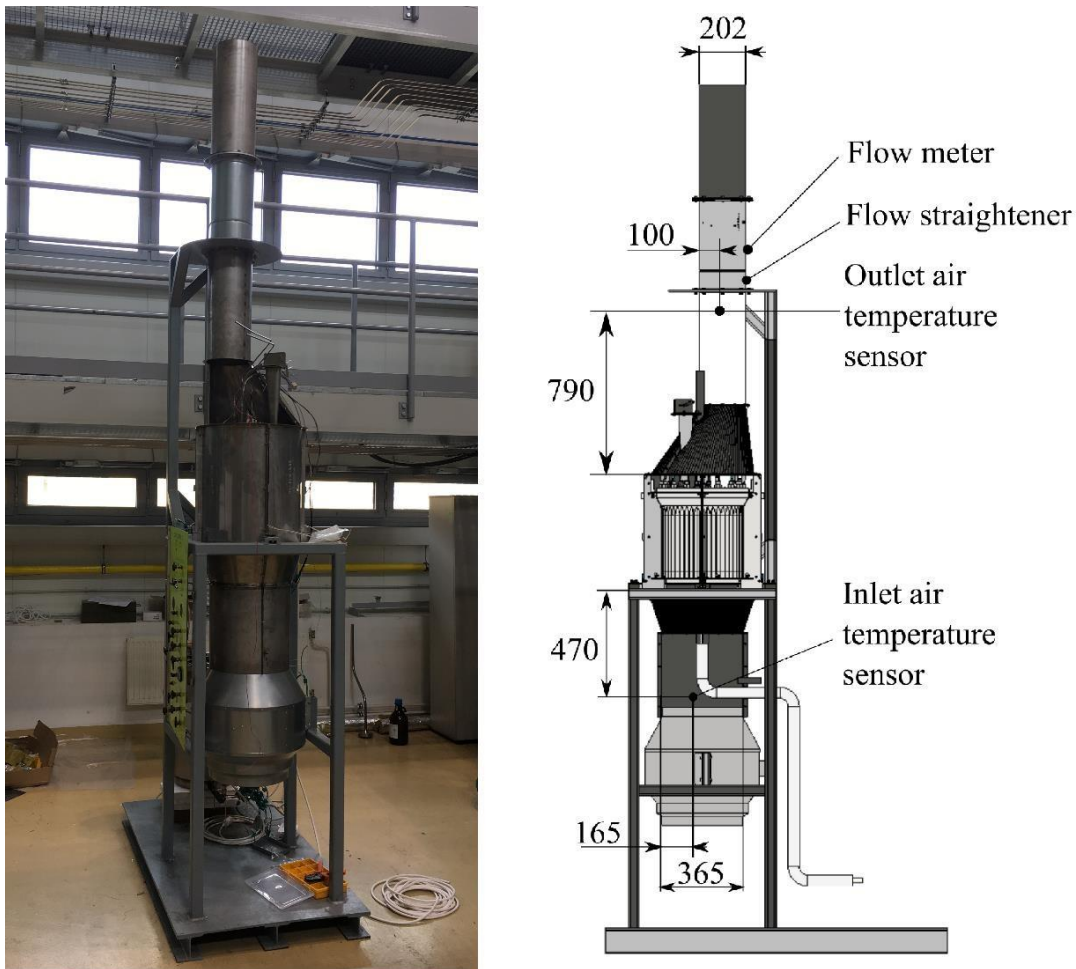


Figure 3-9: The secondary system

3.1.3 The auxiliary system

The auxiliary system includes a water and a gas system. The function of these systems is to provide proper filling and draining of the EV (Figure 3-10). The water system is employed during cooling (clogging) of the draining pipe. The system includes a water reservoir, a piping and a solenoid valve. After the filling of the EV

is finished, the water cools down the lead in the draining pipe close to the SV and therefore plugs the draining pipe. The water is forced from the reservoir by increasing pressure in the reservoir.

The gas system is used to push the liquefied lead from the SV to the EV by increasing pressure in the SV. The other function is to provide a slight overpressure in the experimental rig to prevent contamination by ambient air. The system includes valves, a vacuum pump and high pressure argon and hydrogen bottles. During fast draining of the EV, the pressure is increased in the EV.

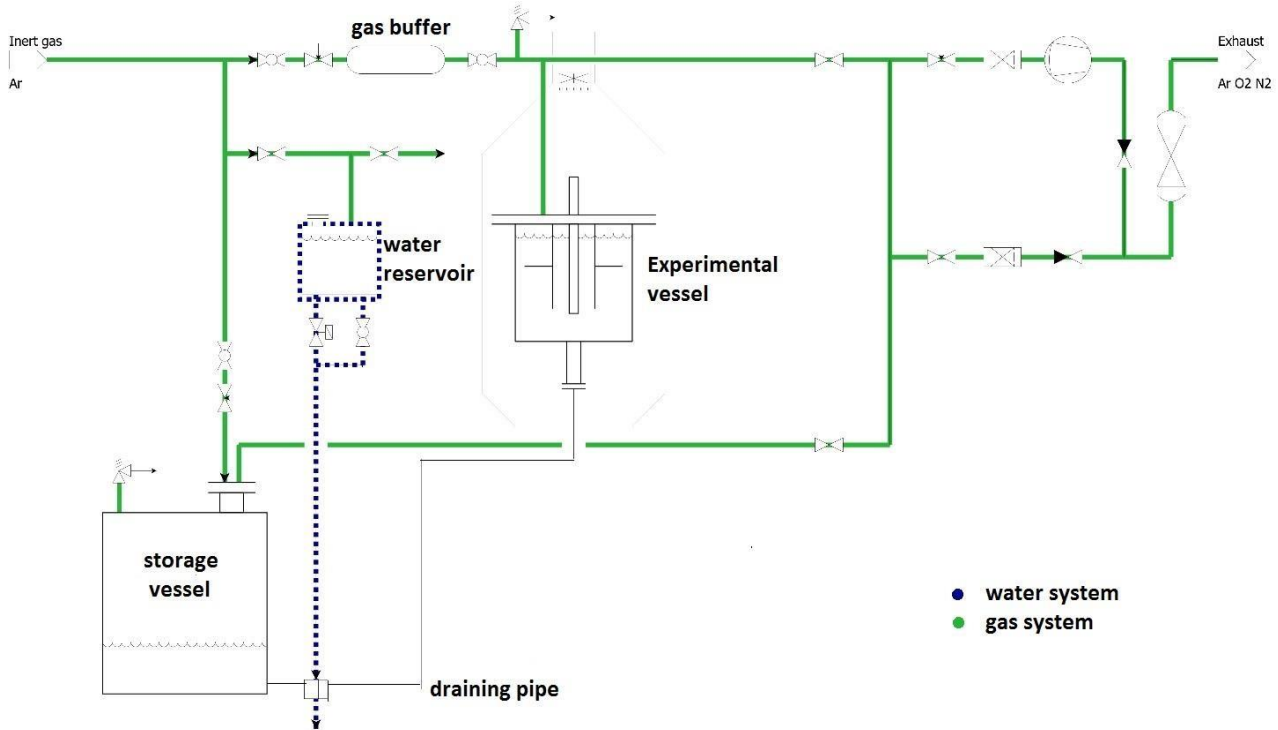


Figure 3-10: The auxiliary system

3.2 Commissioning

Prior to the start of the experiments, several tasks were carried out to ascertain proper and safe operation of the experimental setup. These tasks included TC probe calibration, leak tests, pressure tests, melting and hydrogen purification of the lead and filling of the experimental vessel. Description of the particular operations follows.

TC calibration. The TC probes were designed to meet special requirements by the setup. To ensure that the measured temperature by all TC in the probes was correct, all TC probes were tested in a Gemini 4857 heated block (Isotech Ltd, Merseyside, England) in the range of 100—500 °C. The accuracy of the TC in the probes was ± 2 °C in all measurements.

Leak and pressure tests. Leak tests were carried out prior to the measurements. The primary system was pressurized and soap water was utilized to detect gas leaks. Leaks were detected mostly around the demountable fittings used for the attachment of TC probes. As there was no need to remove the fittings holding the probes, the places around the fittings were welded. This solved the problem and no other leak was found.

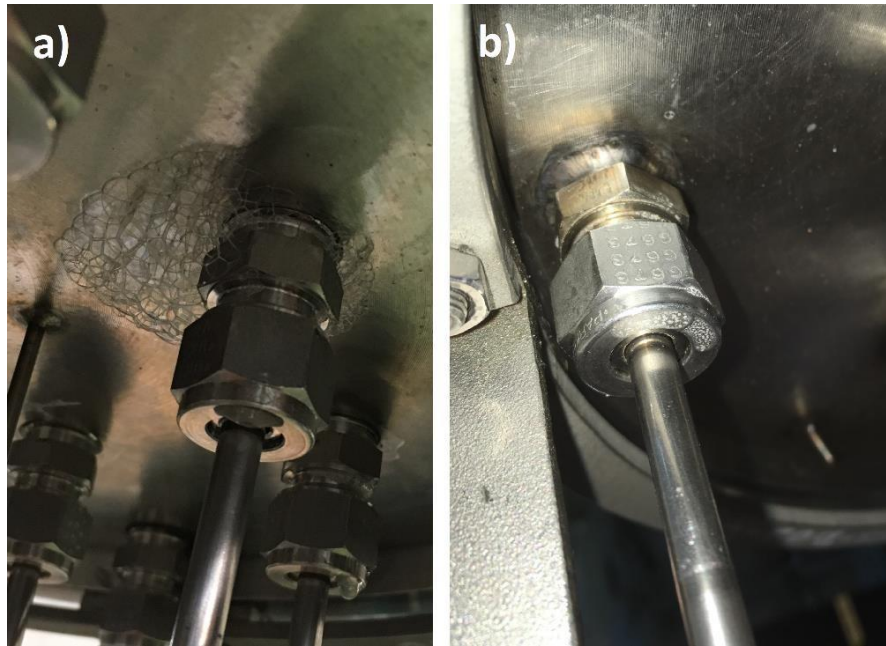


Figure 3-11: Leak tests; a) detected leak, b) welding of the problematic places

The pressure test was carried out after the leak testing (Figure 3-12). The experimental setup was pressurized to 6.3 bar. The pressure was being checked continuously for 1 hour to ascertain that there was no pressure drop in time.



Figure 3-12: Pressure test

Melting and purification. After the experimental setup was checked against the leaks and it was made sure that it could withstand high pressures, the storage vessel was filled with 270 kg of lead in the form of solid blocks. Safety valves were installed above the SV and EV. The whole system was then evacuated using a vacuum pump and filled with pure argon to remove oxygen from the system. This process was repeated three

times. During this procedure, a check of the safety valves, which were set to 3 bar, was carried out to verify their operability. The lead was then liquefied using band heaters attached to the SV.

When the lead content in the SV was melted, an argon/hydrogen mixture in 90/10% concentration was pushed below the lead level for purification purpose and to reduce the amount of oxides in the melted lead. The resulting vapours were sucked out of the vessel. This procedure was ongoing for few hours. After the purification process, the pipe for the mixture was reconnected to the pure argon supply and filling of the EV could start.

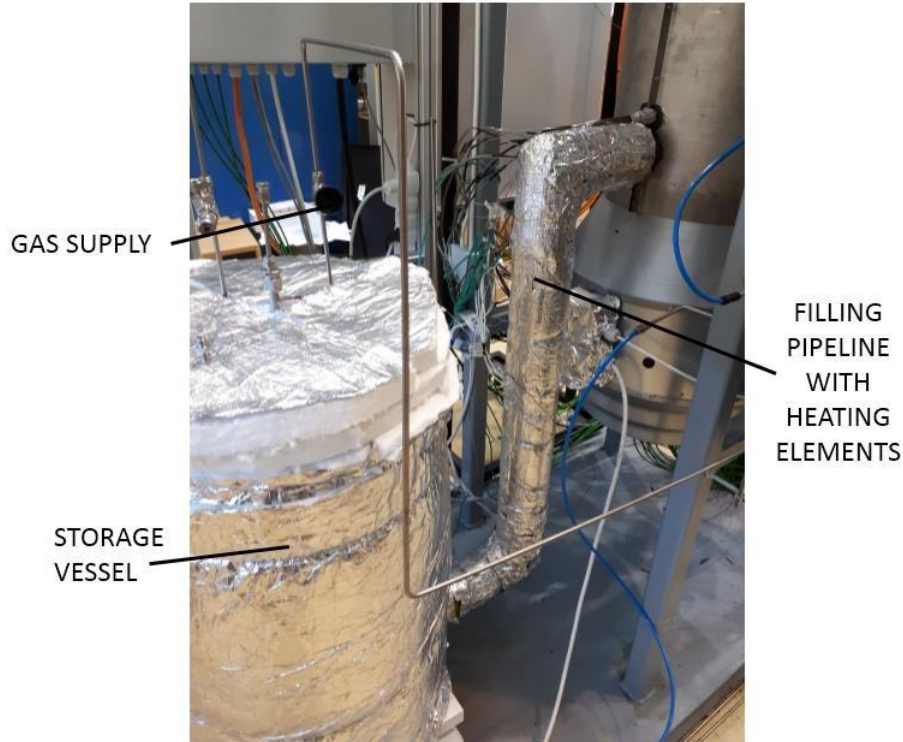


Figure 3-13: Filling pipeline

Filling of the EV. The supply pipeline between the SV and EV as well as the bottom part of the EV were heated to 400°C by heating elements lying on the pipeline under the insulation (Figure 3-13). Filling of the EV from the SV was performed by increasing the pressure in the SV through argon supply. The pressure required to displace the liquid lead in order to fill the EV at the prescribed level was estimated to 1.8 bar. The argon was slowly released into the SV and three parameters were checked: pressure in the SV, lead level in the EV and temperature on the TC probes in the EV. When the lead level in the EV reached the contact level sensor, the valve on the gas supply was closed to maintain the appropriate pressure. Then the heaters on the supply pipeline were turned off to freeze the lead inside and plug the pipeline. At this moment, the fan and the main heaters could be turned on and set to the desired values. Assembly of the whole experimental facility before commissioning process is shown in Figure 3-14.

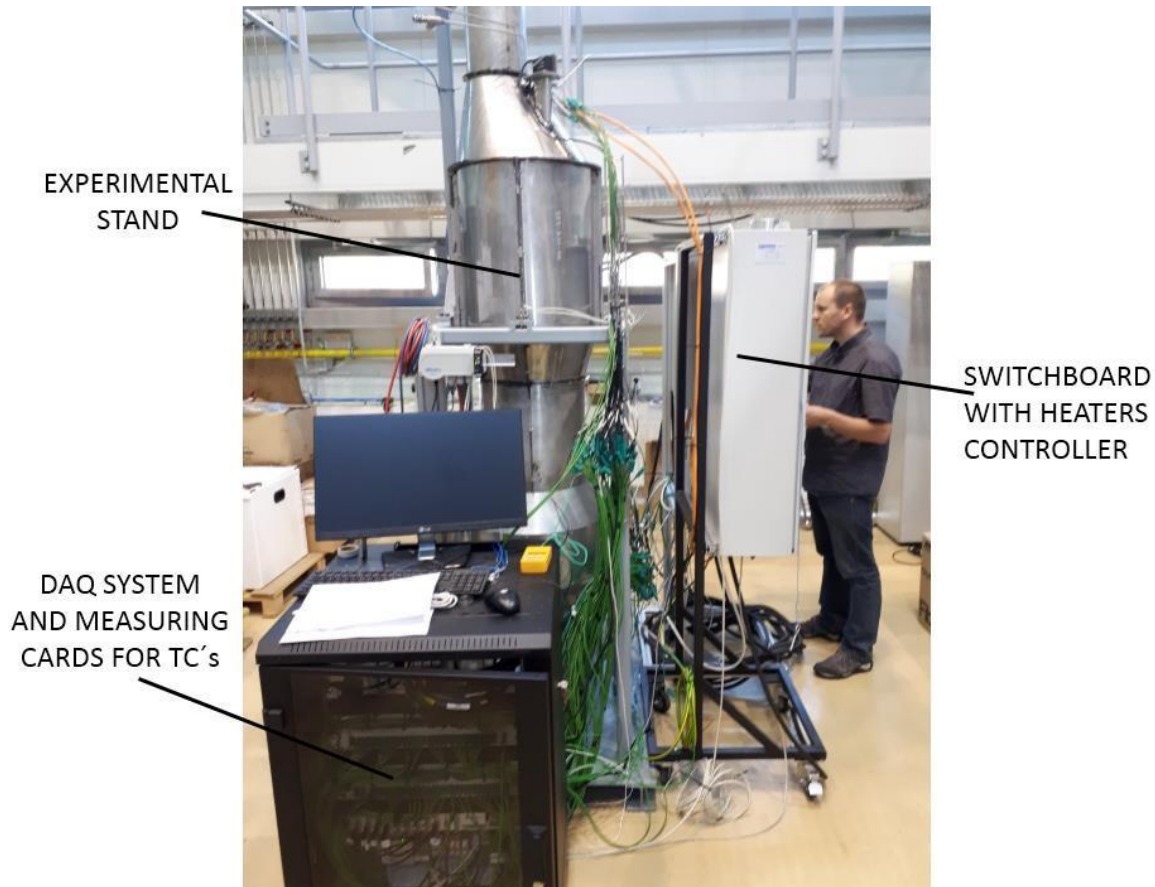


Figure 3-14: Assembly of the experimental stand with auxiliary systems

4 The experimental data

Similarly to the numerical analysis, several steady-states were analysed during the experimental run. These states differed in terms of set heating power and air MFR. The first goal was to reach a state during which all of the lead was liquefied and the minimum lead temperature was above solidification temperature. To do that, the lowest possible air MFR was set and heating power was gradually increased. When the state of liquefied lead was found, the air MFR was gradually increased to evaluate its effect on temperature distribution inside the EV. The results of all conducted steady states can be found in Table 4.

The output of the flow meter system was a value of volumetric flow rate calculated for normal conditions, i.e. atmospheric pressure of 101.325 kPa, air temperature of 20 °C and air density of 1.2 kg/m³. Dynamic pressure was calculated using equations 1 and 2:

$$V = A \cdot v \quad (1)$$

$$p_{dyn} = \rho_{air,20^{\circ}C} \cdot \frac{v^2}{2} \quad (2)$$

where \dot{V} is volumetric flow rate, A is air channel cross sectional area (0.032 m²), v is velocity, p_{dyn} is dynamic pressure, and $\rho_{air,20^{\circ}C}$ denotes air density corresponding to 20 °C. Corrected (real) volumetric flow rate was then calculated with air density corresponding to measured outlet air temperature. This temperature was measured downstream (outlet) of the EV near the Wilson grid (Figure 3-9). The air density at the outlet temperature was obtained from REFPROP version 9 (NIST, Gaithersburg, MD, USA). For simplification, dry air at pressure of 101.325 kPa was assumed. After that, the air MFR was calculated using equation 3:

$$\dot{m} = \rho_{air,outlet} \cdot \dot{V} \quad (3)$$

where \dot{V} is corrected volumetric flow rate and ρ_{air} is air density at outlet temperature. Based on these calculations, the calculated air MFR can differ even though the fan rotation speed was kept constant. The average value over a 5 min period was used for the volumetric flow rate. It is worth noting that the outlet temperature was measured only at one point at the centre of the air channel. A small test was performed during which a temperature profile was measured in one cross section of the air channel. Although the temperature at the centre of the channel was 62.9 °C, the temperatures varied across the channel in the range

of 61.9 and 77.8 °C. Therefore, the temperature measured at the centre of the air channel was an underestimation of the average outlet air temperature. However, the outlet air temperature is used only for the calculation of air density and subsequently air MFR where its effect is minor. Next step will be to properly analyse the outlet air velocity and temperature field in order to find a measurement point that is more accurate in terms of average air outlet temperature than the air channel centre. It is also worth noting that there was noticeable change in ambient temperature in the experimental hall throughout the day. This had to be taken into account while reaching the steady state.

Table 4 Experimental results of steady-states

Case	Air MFR [kg/s]	Volumetric flow rate [m ³ /hod] *	Heating power [kW]	Air inlet temperature [°C]	Air outlet temperature [°C] **	Air density [kg/m ³]	Max TC temperature [°C]	Min TC temperature [°C]
1	0.103	330	3.04	16.8	42.1	1.12	358	254
2	0.102	335	4	19.4	49.0	1.1	371	267
3	0.101	338	4.96	18	56.5	1.07	406	332
4	0.098	346	5.6	20.8	62.6	1.02	435	353
5	0.121	404	5.6	21.3	54.9	1.08	402	329
6	0.145	477	5.6	20.1	50.0	1.09	393	317
7	0.156	511	5.6	20.5	47.7	1.1	378	300
8	0.167	547	5.6	23.5	49.0	1.1	371	287

*Corrected volumetric flow rate for real conditions

**Outlet temperature measured at one point in the middle of the air channel

The temperatures measured by the probes in a cross section of the EV for all the cases can be seen in Figures 4-1 and 4-2 depending on the heating power and the air MFR, respectively. The temperatures measured by the single TCs were included in these figures even though these TCs are not located in the same cross section. This should not have any effect on the results assuming the axisymmetric temperature distribution. The positions of individual probes are depicted in Figure 3-4.

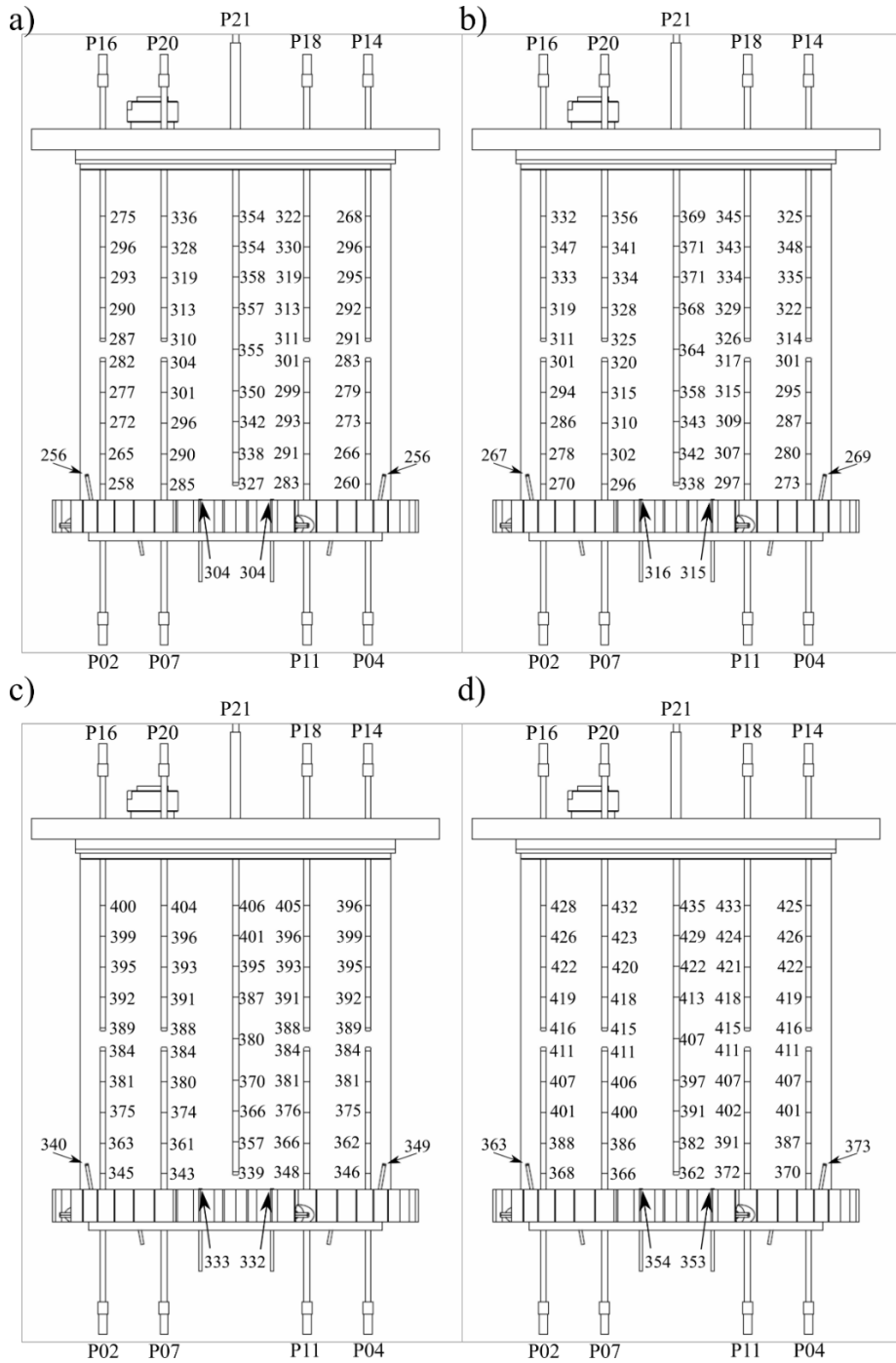


Figure 4-1 Temperature distribution in a cross section of the EV for air MFR of approximately 0.101 kg/s and variable heating power: a) 3.04 kW, b) 4 kW, c) 4.96 kW, d) 5,6 kW

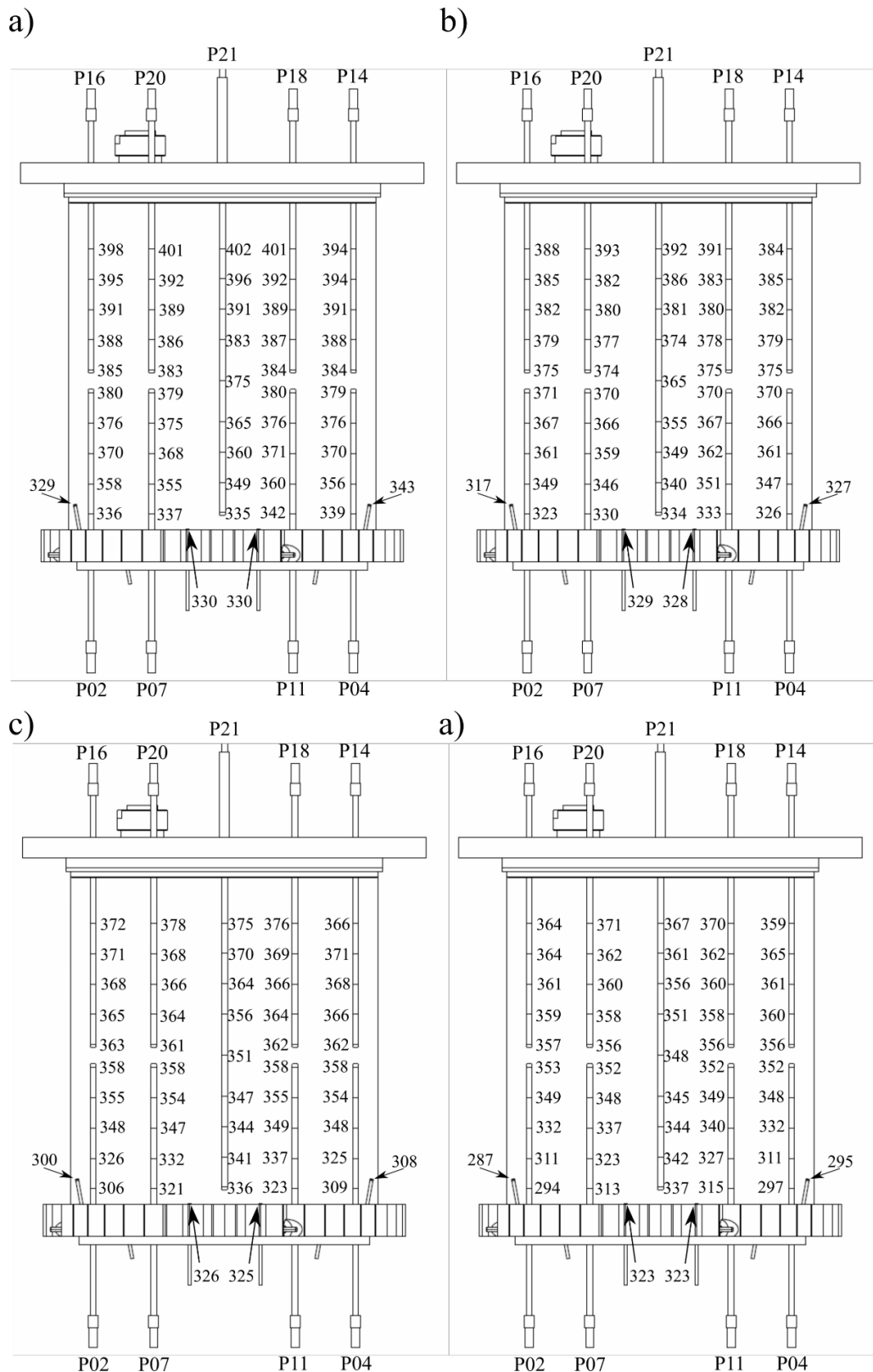


Figure 4-2 Temperature distribution in a cross section of the EV for heating power of 5.6 kW and variable air MFR:
a) 0.121 kg/s, b) 0.145 kg/s, c) 0.156 kg/s, d) 0.167 kg/s

When the minimum air MFR was set (0.095 kg/s), the fully liquid steady state was reached not before the heating power was increased up to 4.96 kW. There is a quite large difference between the experimental and the numerical results. During the numerical simulations, the fully liquid steady state was reached for a heating power of 3 kW and an air MFR up to 0.145 kg/s. It can be concluded that the EV is cooler and the heat transfer

from the EV is larger during the experiments than in numerical simulations. When the heating power in the EV was kept constant at 5.6 kW, the measured temperatures dropped under the solidification temperature for air MFR higher than 0.145 kg/s.

The development of a temperature field between two specific steady states can be seen in Figure 4-3. The temperatures are displayed for two TC probes, probe 2 and probe 16. The air MFR was increased from 0.121 to 0.145 kg/s at time 0. It took almost 300 minutes to reach a steady state in which there was no significant change in temperature. There is also not any noticeable transition from the liquid to solid state as the temperature at TC T0205 dropped from 335 to 320 °C.

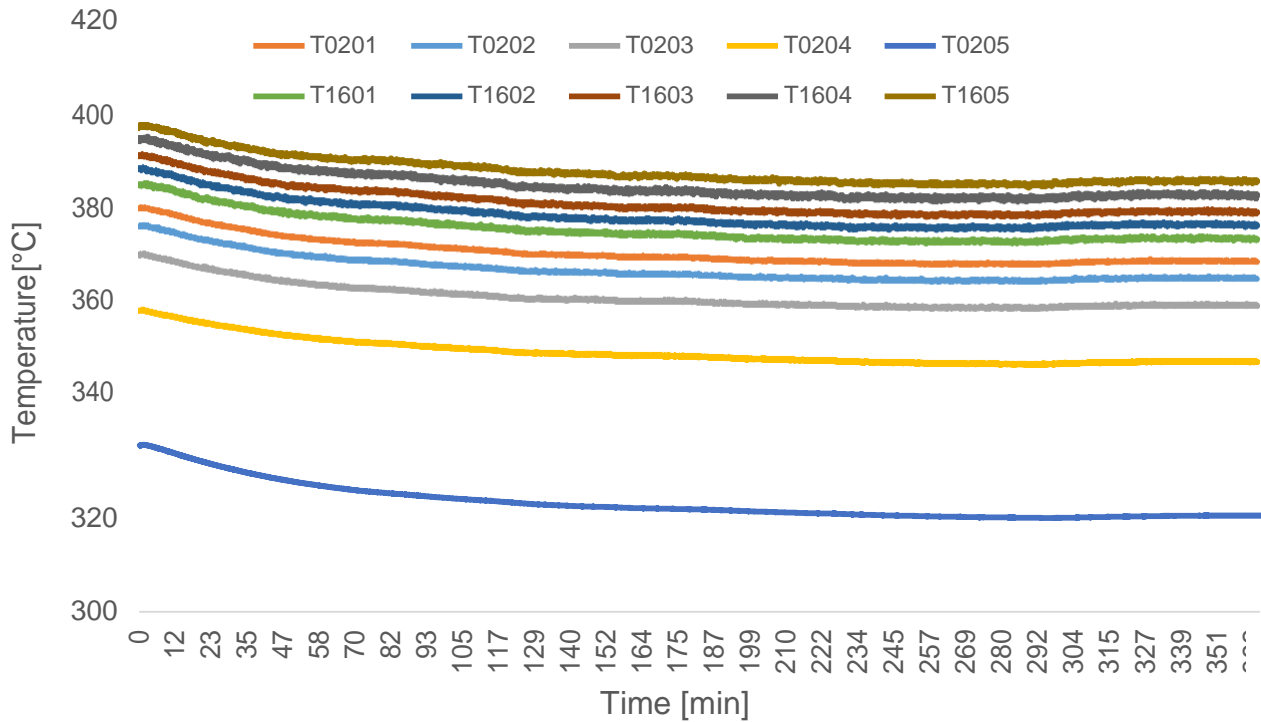


Figure 4-3 Temperature field development after an increase of air MFR from 0.121 to 0.145 kg/s and constant heating power of 5.6 kW

After the last steady state, case 8, was reached, the heating in the SV and in the piping was turned on. The EV was quickly drained leaving the frozen lead fraction at the bottom of the EV. The heating in the EV, in the piping and in the SV was turned off and the experimental setup was cooled down to ambient temperature. After that, the EV was opened and the solidified lead fraction was 3D scanned using a Steinbichler T-Scan CS (Carl Zeiss Optotechnik GmbH, Neubeuern, Germany). The obtained data were analyzed using PolyWorks Viewer (InnovMetric Software Inc., Quebec, Canada) and the shape of the frozen lead structure was measured. The frozen fraction shape in the cross section of the EV is depicted in Figure 4-4. The cross section dividing the EV passes through the probes 8 and 12. The shape of the frozen structure is not displayed all the way to the EV bottom as it was not possible to place the scanner that close. A raw version of the 3D scan can be seen in Figure 4-5.

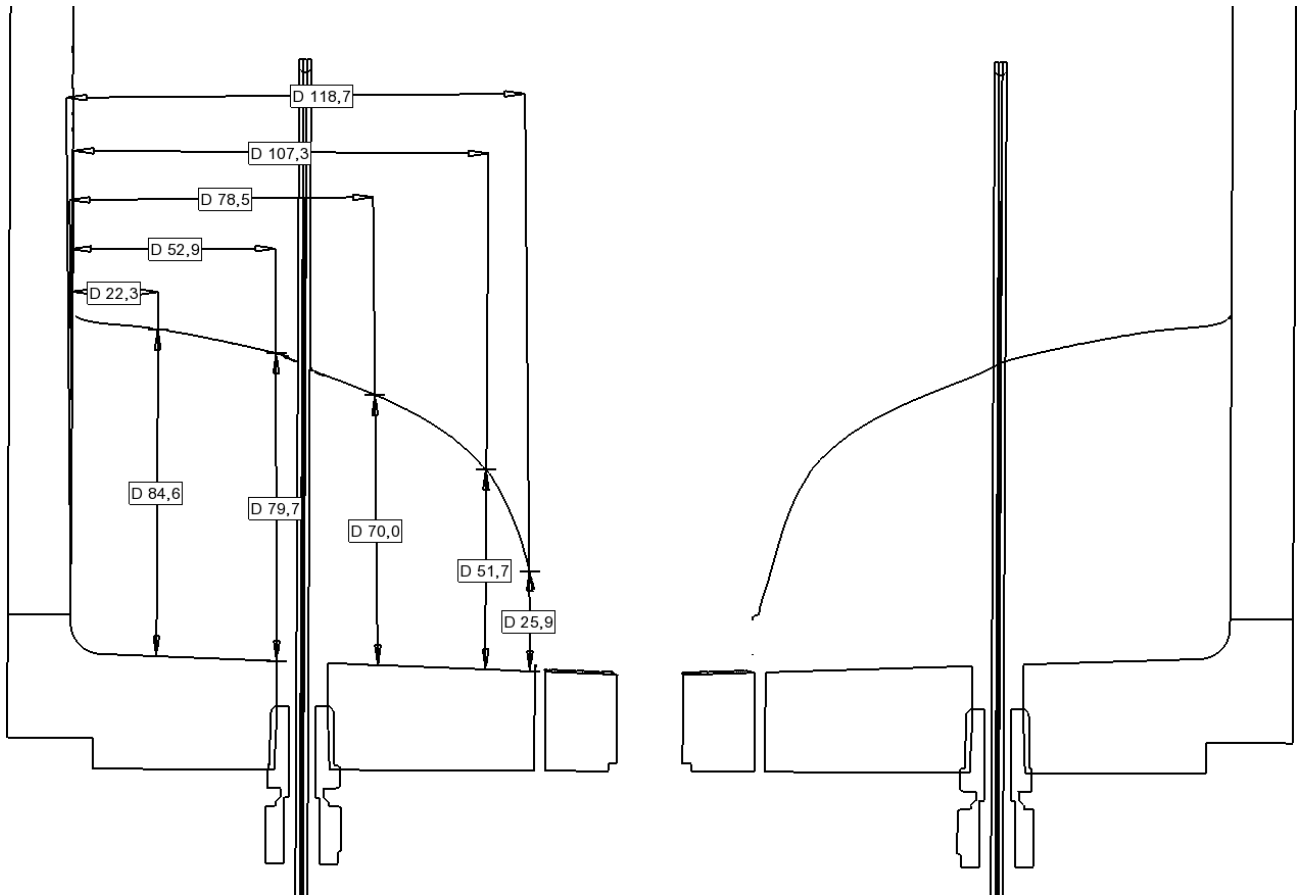


Figure 4-4 A shape of the frozen lead structure during case 8

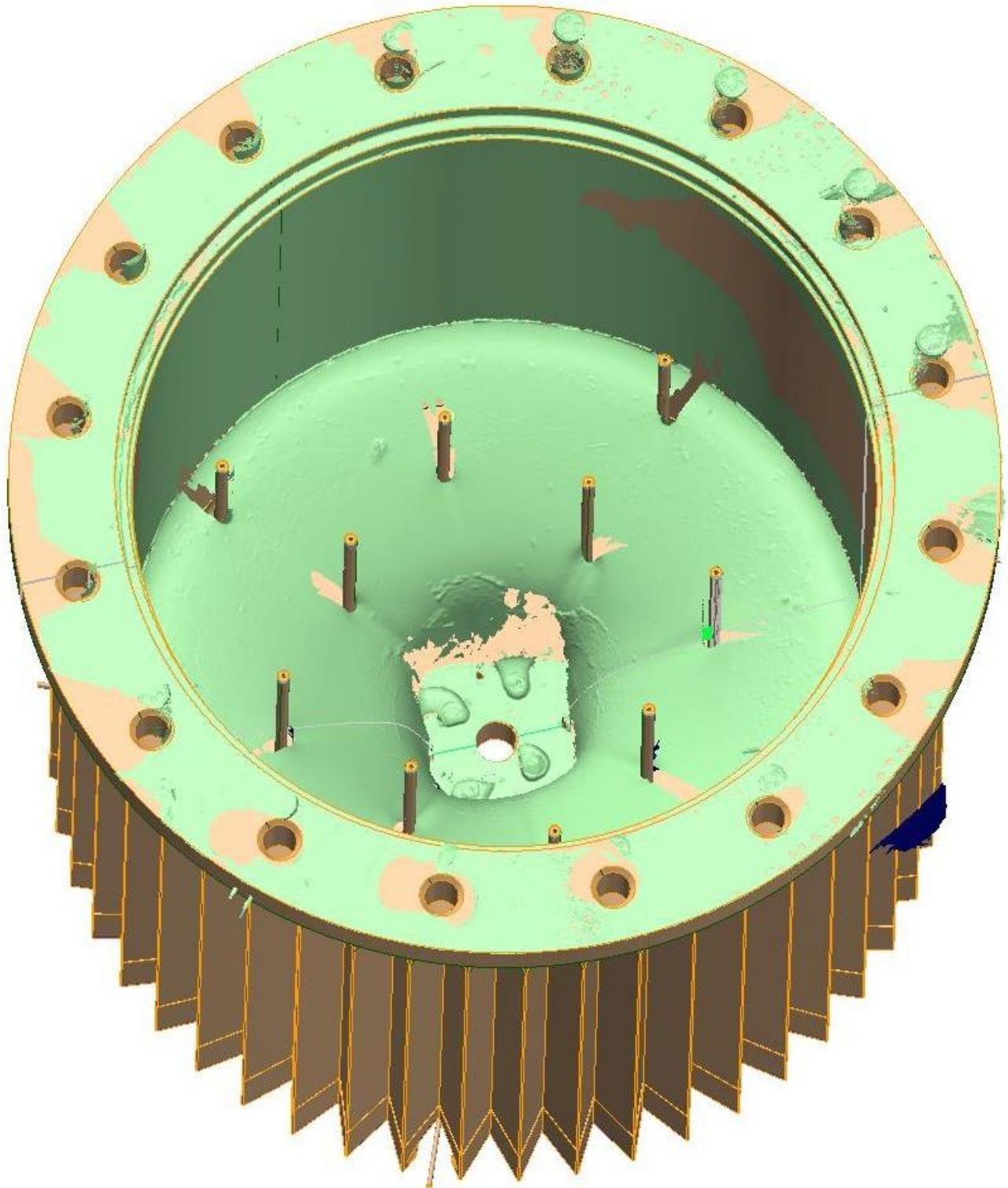


Figure 4-5 The raw 3D scan of the EV with solid lead

5 Conclusions

The experimental setup for the analysis of lead solidification was assembled, tested and commissioned. Several steady states including fully liquid or partially liquid states were analysed and all the boundary conditions, such as air inlet and outlet temperature, heating power and air MFR, were defined. The experimental results indicated that the heat transfer from the EV is larger during the experiments than in the numerical simulations as the measured temperatures were lower for the same operating conditions. However, detailed evaluation of both the experimental and simulated data and their comparison will be a subject of

interest in the forthcoming phase of the activity focused on benchmarking of the computational codes on both steady and transient cases. The time needed for the temperatures to stabilize was very long and it took several hours to transition from one steady state to the other. After the last steady state the liquid lead was quickly drained from the EV and the EV was cooled down by air. The EV vessel was opened and the solid lead was scanned to capture the solidified fraction shape.

The future experimental campaigns are planned to reproduce the experimental measurement and to repeat the measurements with modifications of the geometry (replacement of the internal obstacle, partial blockage of the air channel). Fast transients will be also studied assuming sharp increase of the air MFR to the maximum value to acquire data for validation of the codes ability of prediction of the transient states.

The complete experimental dataset obtained will be released to the SESAME partners under a suitable form for the validation of the computational models.

6 Reference

- [1] O. FRYBORT, I. DOFEK, M. SLINC a J. VIT, Description of the Meliloo - stand test facility and test matrix, H2020 SESAME project deliverable (654935), 2016.
- [2] R. Kent Dybvig, The Scheme Programming Language, The MIT Press, 2009.
- [3] FLUENT 17.0 User's Guide, ANSYS, 2017.
- [4] F. REOLOFS a e. al., Status and Perspective of Turbulent Heat Transfer Modelling for the Industrial Application of Liquid Metal Flows., Nuclear Engineering and Design 290 (2015) pg. 99-106, 2015.
- [5] B. NICENO a A. BADILLO, Summary for the Recommended Physical Properties for the Main Fluid and Liquid Materials Used for the MELILOO-stand and TALL-3D Freezing Experiments Version 1.0, Paul Scherrer Institute, H2020 SESAME project deliverable, 2016.
- [6] NIST - REFPROP version 9.0.
- [7] 321 Stainless Steel Data Sheet, revision 04.25.13, AK Steel Corporation.
- [8] KANTHAL A1 Datasheet, <https://www.kanthal.com/en/>.

7 Appendix – CFD model of CRS4

Summary

Pre-test simulations of the SESAME-Stand experimental facility constructed at CVR have been performed in STAR-CCM+ for the development of a solidification model with liquid lead as working fluid in the pool and air in the cooling channel. The thermal equilibrium is reached in steady state. Increasing the mass flow rate in the cooling air channel, the solidification procedure is initiated and the freezing front propagates in the pool until reaching the internal obstacle. The numerical results are compared with the CVR results showing good general agreement.

Table of contents

1	Introduction	29
2	Sesame-Stand facility. Computational model	30
2.1	Geometry	30
2.2	Surface and volume mesh	31
2.3	Physical properties and numerical models	32
2.3.1	Liquid/solid lead domain	33
2.3.2	Solid domains	33
2.3.3	Argon domain	33
2.4	Thermocouples distribution.....	34
3	Solidification model	34
3.1	Numerical set-up for thermal equilibrium	34
3.2	Solidification setting and numerical issues	37
4	Simulation results.....	38
4.1	Steady-state results	38
4.2	Transient results	41
4.3	Technical issues about variable density flow in STAR-CCM+.....	43
5.	CONCLUSIONS.....	44

1 Introduction

The development and the validation of computational models able to simulate the liquid metal thermal-hydraulic and the relative freezing phenomena are essential for the development of liquid metal cooled Gen IV reactors and for their safety assessment. For this purpose, activities focused on development and validation of computational models simulating the liquid lead natural convection and freezing are being performed within the H2020 SESAME project. The first step of this work package is to develop a suitable computational model, which will be then validated by the experimental data obtained from an experimental stand, which will be operated at CVR in the next phases. In this sense, in the framework of the WP3, a collaboration with the CVR partners has been set-up for the comparison of the numerical and experimental work performed on the SESAME-Stand experimental facility. The CRS4 work is dedicated at this stage to the modelling of the pool region of the experimental stand for pre-test analysis.

A full 3D numerical model of the SESAME-Stand test section has been built in STAR-CCM+[1], progressively improved and appropriately instrumented. The CFD model has been constantly compared with the experiment design described in the SESAME-Stand reference document (Deliverable 3.8-Meliloo setup [2]) and with the

similar CFD model developed at CVR with the FLUENT software [3]. The construction of the numerical model has taken only progressively all the features of the real experimental setting.

Steady-state simulations are set up using input (heat source, cooling air mass flow rate) from the experimental work ongoing at CVR. The global thermal equilibrium is obtained and the system is brought to the desired temperature close to the freezing onset. Increasing the cooling air mass flow rate, the solidification process is initiated. The simulation of the freezing is done both in steady state and transient state activating the Melting-Solidification model, sub-model of the Volume of Fluid (VOF) Eulerian multiphase framework.

The first main outcome of the simulation is an important difference in the temperature field between the two numerical models. The same minimum temperature near the freezing point is obtained for a higher heat source in our model: the CVR heat source is fixed at 3 kW while in STAR-CCM+ the heat source must be 3.12 kW. With this difference accepted, the steady state results obtained with the two codes are comparable while the transient results indicate that the same percentage of solid lead is reached faster in the CVR's model.

The thermal stratification is well captured by fixing the reference density in the lead domain to the effective density of the lead. The velocity field is not well captured by STAR-CCM+. In a simplified test case, with only one liquid lead domain and temperature fixed at the wall, the velocity is correctly resolved but not in the case of the complex geometry with the temperature controlled by the cooling air flow rate.

The geometrical model and the physical properties of the materials involved in the numerical model are illustrated in Section 2. The description of the solidification model and the related numerical issues are given in Section 3. The numerical steady state and transient results are illustrated in Section 4.1 and Section 4.2, followed by an analysis of the technical issues faced in STAR-CCM+ in Section 4.3. The conclusive analysis is made in Section 5.

2 Sesame-Stand facility. Computational model

2.1 Geometry

The 3D geometrical model was built with the STAR-CCM+ 3D-CAD modeler, according to the sizes indicated in the deliverable D3.8 issued by CVR. The CFD model includes the experimental vessel and the cooling air duct. The experimental vessel is formed by:

- Solid walls
- Fins in the form of triangular ribs for larger heat transfer area
- Main Heater
- Pipes for the thermocouple probes
- Inner obstacle
- Fluid: Lead
- Fluid: Argon
- Numerical Argon Top Outlet
- Bottom plug

These parts form the CFD domain and they will be described briefly in this section. The description follows the order in which the geometrical parts have been constructed and is illustrated in the pictures in Fig. 1.

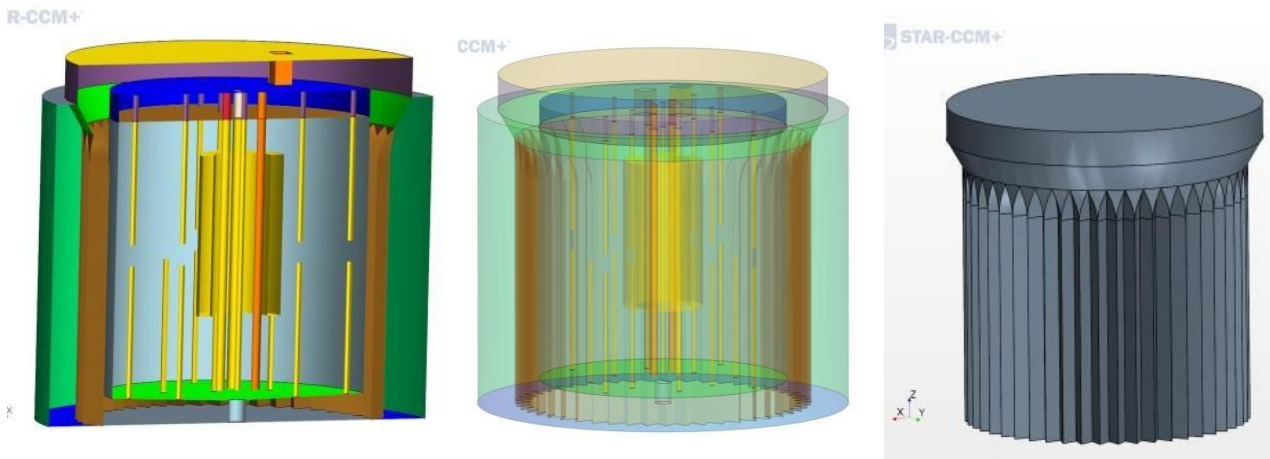


Fig. 1: Geometry of the computational model

The lateral walls, the bottom and the top parts of the vessel were built together by a 360 degrees revolution of the corresponding 2D profile. The vessel's bottom accommodates the plug for the draining pipe for the liquid lead and for this reason it was designed to help the lead's flow with 2° of inclination.

The characteristic dimensions of the vessel are:

- o Inner diameter = 300 mm
- o Outer diameter = 360 mm
- o Height = 404 mm

The cooling air channel has the following characteristic dimensions:

- Inner diameter = 320 mm
- Outer diameter = 450 mm
- Height = 300 mm.

The heater is formed by four heating rods placed in the center of the experimental vessel, around the central thermocouples pipe. The heating rods are simple steel cylinders with the outer diameter of 10 mm.

There are 12 bottom pipes and 8 top pipes inside the pool which host the thermocouples. They have a 6 mm diameter a length of 200 mm. In the numerical model, the four pipes hosting the thermocouples have a hexagonal geometry instead of circular, for better mesh matching at the interfaces with the fluid.

An internal obstacle is inserted to guide the natural circulation of the liquid lead. The obstacle has cylindrical shape.

The lead domain is a cylinder with the diameter of 300 mm and the height 300 mm. The fluid volume is obtained by subtracting from the cylinder all the solids.

The argon volume occupies the upper part of the vessel's internal for 40 mm of height above the lead volume. In the experiment, the argon layer is meant to compensate the volumetric expansion of the lead and to avoid air penetration in the vessel.

2.2 Surface and volume mesh

Once the geometrical parts have been assigned to the regions and the interfaces between the various solids-fluids, solid-solid, fluid-fluid regions have been defined, the surface and volume mesh have been generated. In STAR-CCM+, the mesh operations have been transferred from regions to the geometrical parts levels. Here, different mesh operations can be defined for different geometry parts. The interface assure the continuity between the adjacent regions, although not conserving the mesh conformity when different regions are meshed with different operations.

The meshers used in the simulation are the Surface Remesher and the Polyhedral Mesher. For the fluid region, the Prism Layer Mesher is added. The sizes of the mesh are the following ones:

- Surface size: 2-4 mm
- Prism layer thickness in the fluid domain: 2 mm
- Total volume mesh representation: 2.8 million of control volumes (illustration in Fig. 2 and Fig. 3).

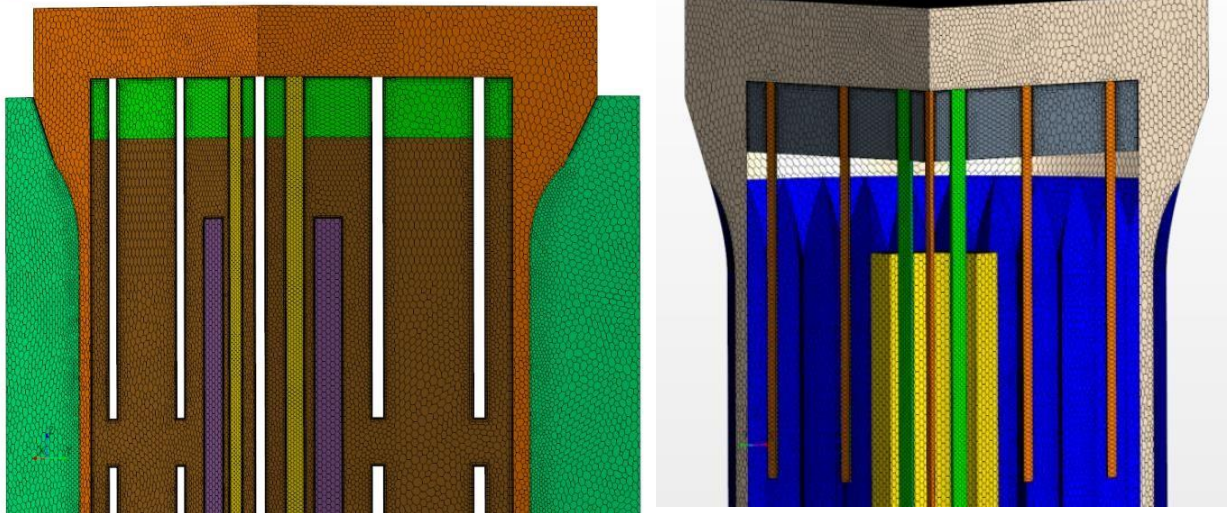


Fig. 2: Volume mesh in the complete geometrical domain, distinguished by regions

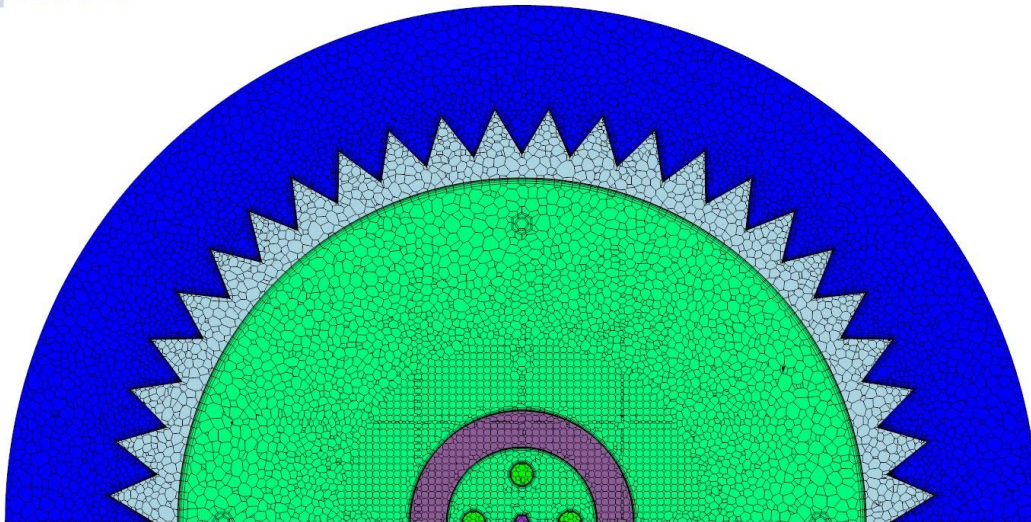


Fig. 3 Volume mesh on a transversal section of the half domain

2.3 Physical properties and numerical models

The following physical models are set up in the numerical simulation for the fluid domains (lead, argon, air):

- Time: Steady/Unsteady
- Material: Liquid
- Flow: Segregated Flow
- Equation of state: Polynomial Density/Constant Density
- Viscous regime: Turbulent; Reynold-Averaged Navier-Stokes
- Reynold-Averaged Turbulence: K-Epsilon Turbulence, Realizable K-Epsilon Two-Layer, Two-Layer All y+ Wall Treatment
- Segregated Fluid Temperature
- Gravity

For the solid domains, the following physical models are set up in STAR-CCM+:

- Time: Steady/Unsteady
- Material: Solid
- Equation of state: Constant Density
- Segregated Solid Energy

The physical properties of the fluids and solids involved were set up according to properties recommended in [4] and they are reported below for the sake of completeness.

2.3.1 Liquid/solid lead domain

The working fluid in the vessel is the molten lead. The physical properties of the liquid lead are listed in

Table 5. The thermo-physical properties of the lead in solid state are given in Table 6.

Table 5: Liquid lead properties

Property	SI unit	Correlation	Temp. range (K)
Density	kg/m ³	$\rho = 11441 - 1.2792T$	$T_M - 1900$
Heat capacity at constant pressure	J/kg-K	$c_p = 176.2 - 4.923 \times 10^{-2}T + 1.544 \times 10^{-5}T^2 - 1.524 \times 10^{-6}T^{-2}$	$T_M - 1300$
Dynamic viscosity	Pa-s	$\mu = 4.55 \times 10^{-4} \exp(1069 / T)$	$T_M - 1500$
Thermal conductivity	W/m-K	$k = 9.2 + 0.011T$	$T_M - 1400$

Table 6: Solid lead properties

Property	SI unit	Correlation (K)	Temp. range (K)
Heat capacity at constant pressure	J/kg-K	$C_p = 126.49 + 4.7 \times 10^{-2}(T - 273.15)$	$300 - T_M$
Thermal conductivity	W/m-K	$k = 30 - 17.3 \times 10^{-3}(T - 600.6) = 40.39 - 17.3 \times 10^{-3}T$	$80 - T_M$

2.3.2 Solid domains

The vessel walls, the thermocouples pipes and the heater are made of stainless steel with the following physical properties, listed in Table 7. The heater consists in a unique solid region to which a numerical heat source is applied.

Table 7: Physical properties of stainless steel

Property	SI unit	Correlation	Temp. range (C)
Density	Kg/m ³	$\rho = 8090$	
Heat capacity at constant pressure	J/kg-K	$C_p = 500$	$0 - 100$
Thermal conductivity	W/m-K	$k = 14.5 + 0.015T$	$100 - 500$

2.3.3 Argon domain

The Argon has the following thermal properties, listed in Table 8:

Table 8: Physical properties of Argon at 1 bar

Property	SI unit	Correlation	Temp. range (K)
Density	Kg/m ³	$\rho = 4.5751 - 1.57317 \times 10^{-2}T + 2.32033 \times 10^{-5}T^2 - 1.24240 \times 10^{-8}T^3$	$273 - 700$

Heat capacity at constant pressure	J/kg-K	$C_p=521$	273 – 700
Thermal conductivity	W/m-K	$k = 1.55271 \times 10^{-3} + 5.96287 \times 10^{-5}T - 1.92121 \times 10^{-8}T^2$	273 – 700
Viscosity	Pa-s	$\mu=1.82652 \times 10^{-6} + 7.69524 \times 10^{-8}T - 2.51082 \times 10^{-11}T^2$	273 – 700

2.4 Thermocouples distribution

The computational model is instrumented with a series of thermocouples with the following distribution, shown in Fig. 4:

- 12 TC probes -Pitch 25 mm- at the bottom of the vessel
- 8 TC probes –Pitch 10 mm – at the top of the vessel
- 1 TC at the center of the vessel
- 4 single thermocouple probes near the heater
- 4 single thermocouple probes at the bottom, on the vessel's wall

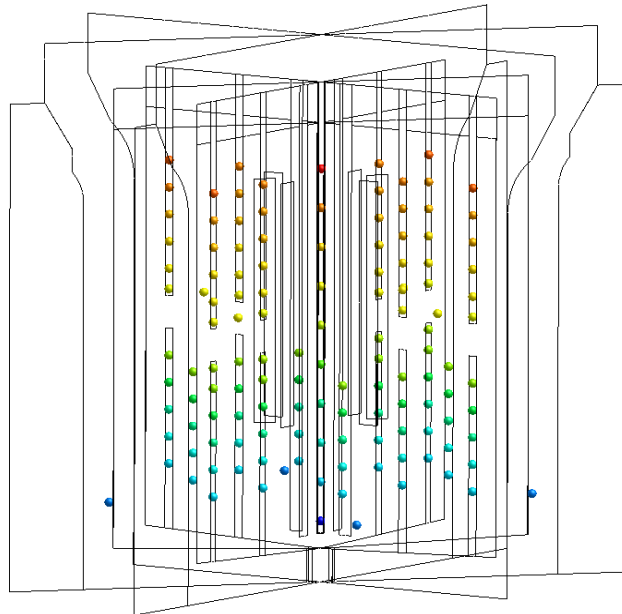


Fig. 4: Distribution of the thermocouples in the vessel

3 Solidification model

In STAR-CCM+, the access to the Melting-Solidification model is giving once the Volume of Fluid (VOF) model is enabled in an Eulerian multiphase configuration with Lead as single phase. The Argon zone at the top of the lead is treated as a separated fluid continuum connected with the lead continuum by means of a baffle interface.

The numerical model doesn't have an inlet for the lead domain, the volume fraction of lead occupying the full closed domain where the natural circulation and the freezing are simulated.

The cooling air duct has a velocity inlet at the bottom and a pressure outlet at the top.

The heat transfer between the outlet and the inlet of the air is measured and monitored.

3.1 Numerical set-up for thermal equilibrium

The algorithm used to bring the system to the thermal equilibrium close to freezing onset is the following one:

- Impose the cooling air velocity and temperature

- ii. First guess of the heat source based on the heat flux removed by the air
- iii. Reach the steady state solution
- iv. Look at the minimum temperature of the lead
- v. Adapt dynamically the heat source to bring the global enthalpy content to the value that provides the right minimum temperature

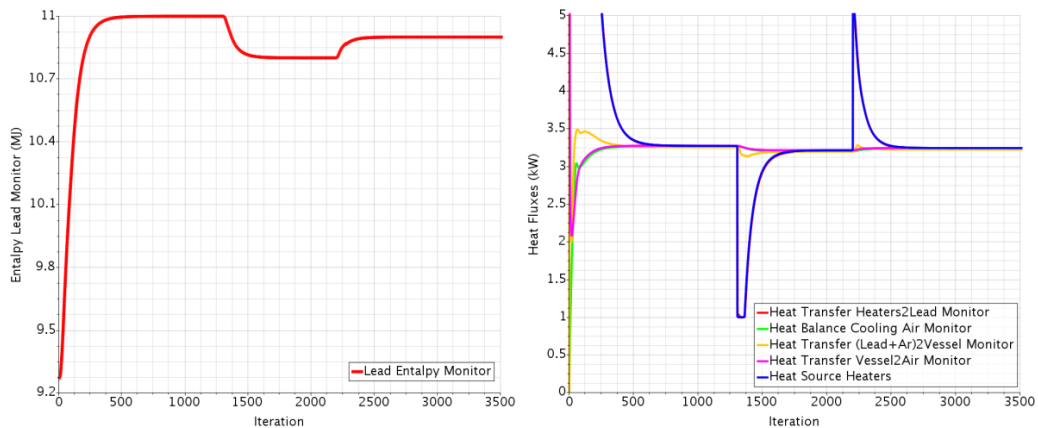
$$HS = \min(20 \text{ kW}, \max(HF - 0.01 * (H - H_0), 1 \text{ kW})),$$

where

HS is the heat source,
 HF is the heat flux removed by the cooling air,
 H is the total enthalpy of the lead,
 H₀ is the target enthalpy of the lead.

- vi. Fix the new found heat source to a constant value

The algorithm is necessary because the steady' state minimum lead temperature is very sensitive to the heat source value. The above procedure bringing the system to the desired minimum temperature near the solidification point is illustrated by means of the monitors plots shown in Fig. 5.



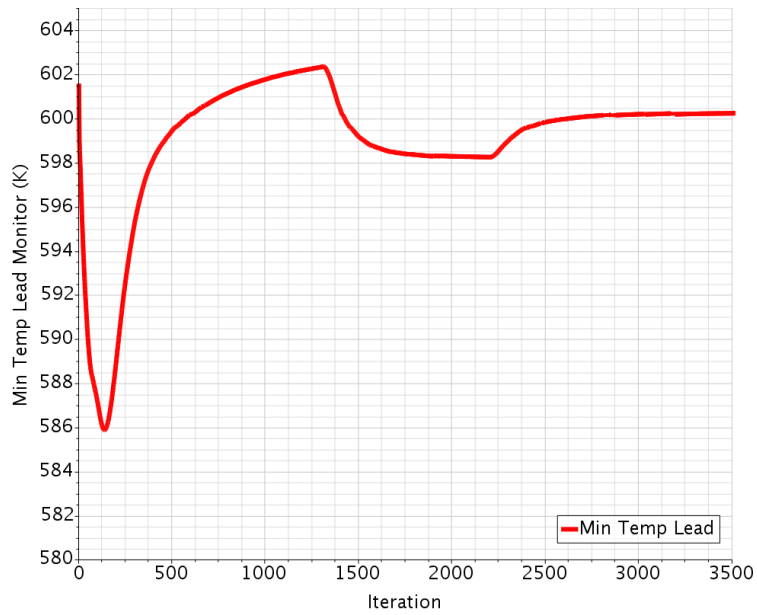


Fig. 5 Thermal equilibrium of the system

The Reference Density, is by default in the VOF framework the density of the lightest phase, in our case, the cover gas density. Imposing the reference density to 1 kg/m³, the temperature profile doesn't show the expected horizontal stratification. The increment of the reference density from 1 to 1000 kg/m³ does not change the temperature and velocity profile. Moreover, the velocity field is not resolved. In the lower zone of the heater, higher temperatures are present and consequently, higher velocities, as shown in the pictures in Fig. 6.

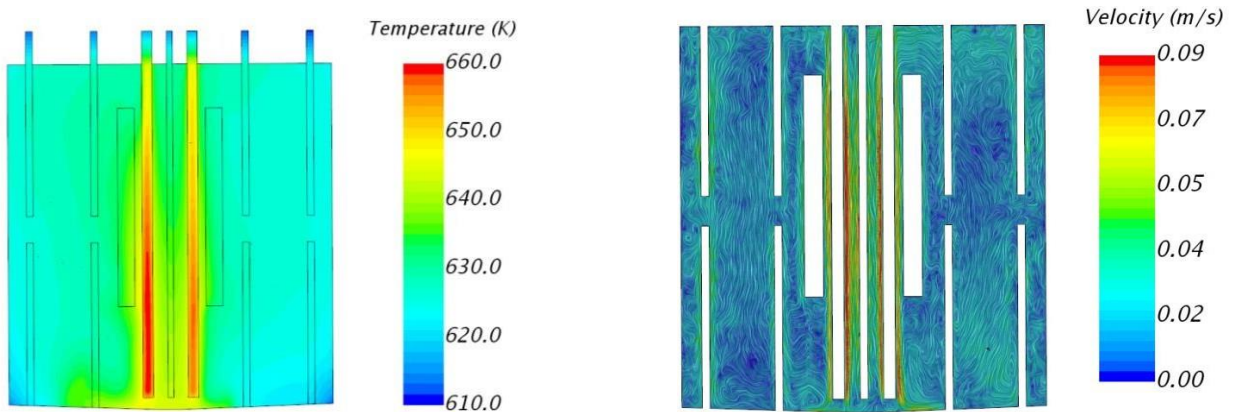


Fig. 6: Temperature and velocity fields in the case with reference density 10 kg/m³

The temperature profile shows the expected horizontal stratification when the reference density is fixed in the order of the lead density, 10000-10700 kg/m³. The lead heated in the internal of the obstacle rises up to the top, then is cooled and turns back (Fig. 7, Fig. 8).

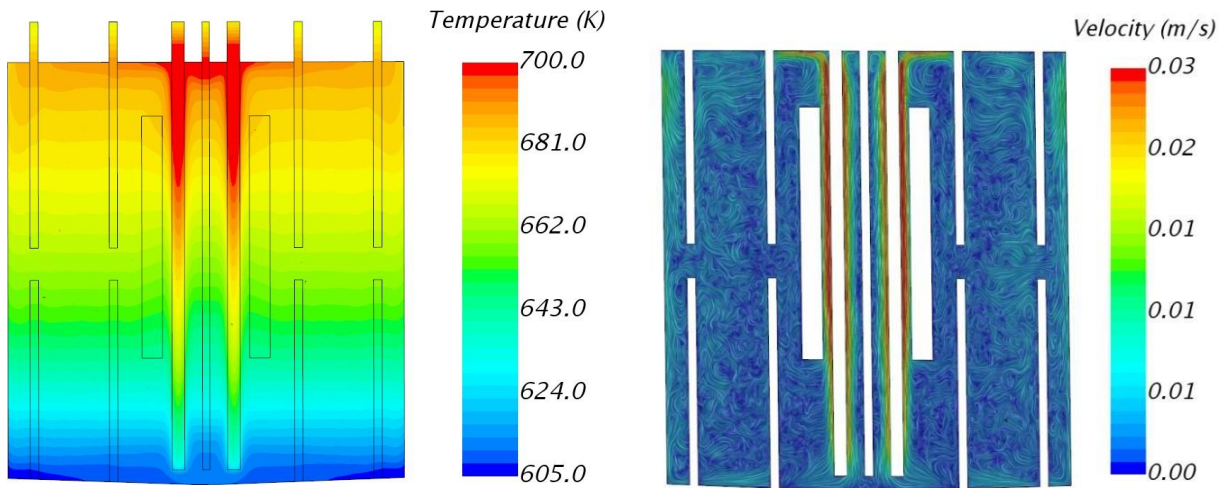


Fig. 7 Thermal stratification and velocity field in the liquid lead domain with reference density 10700 kg/m³

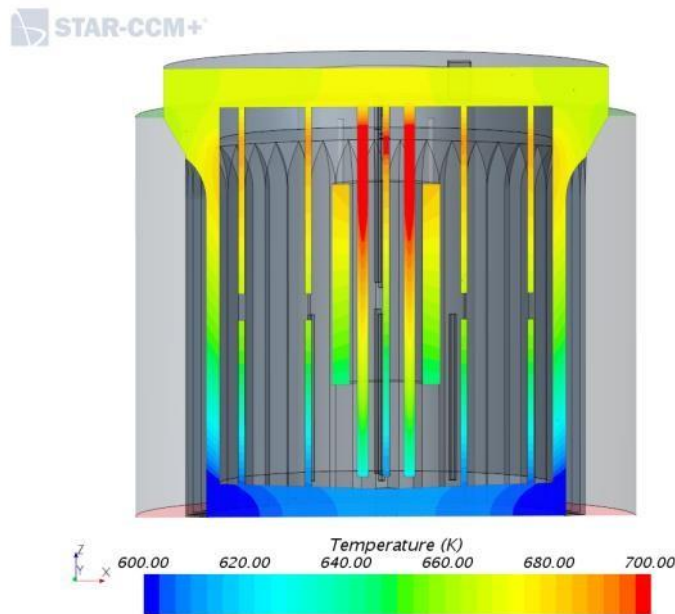


Fig. 8 Thermal stratification on the section across the solids

3.2 Solidification setting and numerical issues

The minimum temperature of 601 K is reached for a heat source of 3.12 kW. In the Volume of Fluid framework, the Melting-Solidification model is enabled with the following settings:

- Latent heat of fusion=23070 J/kg
- Liquidus temperature=600.6 K
- Solidus temperature=598.6
- Flow stop relative solid fraction=0.01
- A low Turbulent Prandtl number (10^{-6}) where the Flow Stop Flag > 0.5 and the default Prandtl number =0.9 otherwise

The simulation is run in steady state, both in the initial liquid lead phase and in the solidification phase. The melting-solidification model is activated when the temperature reaches 601 K or below, by increasing the velocity of the air in the cooling channel.

In the case with the reference density fixed in the range 1-1000 kg/m³ the solidification proceeds well, but incorrect temperature and velocity fields are obtained.

In the case with high reference density (10000 kg/m^3), the simulation diverges brusquely once the temperature is lower than the solidification point, seemingly for the high values of the turbulent dissipation rate in the cells where the freezing initiates.

The strategy to prevent the divergence consisted initially in reducing the convergence tolerance of the solvers, both velocity and pressure; however, the enhancement of the convergence did not avoid the divergence. The divergence was avoided by switching the steady state simulation just before the beginning of the solidification to the transient setting and initiate the solidification in transient for a short time (about 100 s). At this stage, the transient simulation can start with a small time step and a large number of inner iterations and with smaller under relaxation factors in the velocity and pressure solvers. Further on, the time step is progressively increased, the inner iterations diminished and, since the transient run is quite slow, the simulation is switched back to steady state, the delayed freezing is recovered and the solidification front advances normally.

A quarter of the computational domain was considered in order to reduce the computational time and to be able to proceed with the transient for a more meaningful simulation of the freezing phenomena.

4 Simulation results

In agreement with the CVR partners, the steady state calculations have been performed with the aim to find both the optimal initial and final working conditions for the experimental runs. The desired initial condition consists of two goals: a minimum temperature close to the freezing point and a heating power able to provide a fast transient to the freezing of the Lead volume. A general hypothesis was agreed and assumed: during both steady state and transient calculations, only the cooling air mass flow rate must be modified to make the results easily understandable.

4.1 Steady-state results

For the initial condition, an air mass flow rate of 0.145 kg/s and a heating power of 3 kW were chosen at CVR. In the CRS4's model, for the same mass flow rate of the cooling air, the minimum temperature above the freezing point (601 K) is reached for a heat source of 3.12 kW . The heat source difference could be caused by the geometrical difference between the two models.

An interesting final state for an experimental run was found by CVR for 0.176 kg/s of cooling mass flow rate and 3 kW of heating power: the solidification front arrives very close to the internals (heaters and obstacles) without reaching them. This allows the operators to open the vessel and to scan the solidification front. Similarly, in the CRS4's model, this condition is reached for a mass flow rate of 0.178 kg/s and the heat source of 3.12 kW .

The steady state results obtained in the STAR-CCM+ simulations in the two cases are illustrated below. The velocity and temperature fields are shown in Fig. 9 in the case of 100% molten lead and in Fig. 10 and Fig. 11 in the case of the higher cooling air velocity (providing 33% of frozen lead). In Fig. 12, the general thermal behaviour (both in the initial and final steady state conditions) is illustrated by means of significant plots showing the solid lead volume and percentage, the heat flux, the minimum lead temperature and the total enthalpy of the lead.

Case 1. Air velocity= 1.8 m/s (MFR= 0.146 kg/s), heat source= 3.12 kW , lead enthalpy= 2.64 MJ , Minimum lead temperature= 601 K

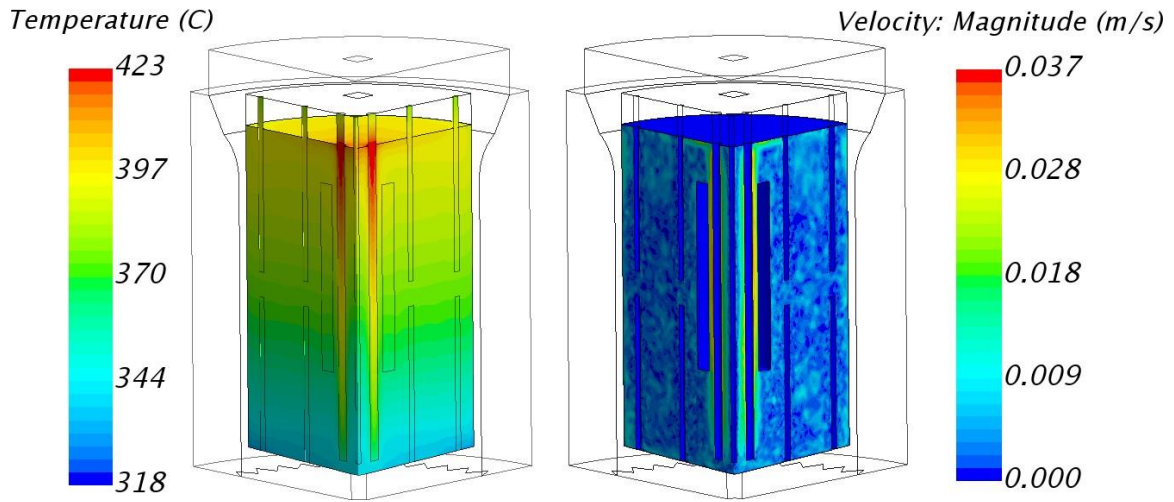


Fig. 9: Temperature and velocity fields in case of 100% molten lead

Case 2. Air velocity=2.2 m/s (MFR=0.178 kg/s), heat source=3.12 kW, lead enthalpy=2.3 MJ, Minimum lead temperature=550K

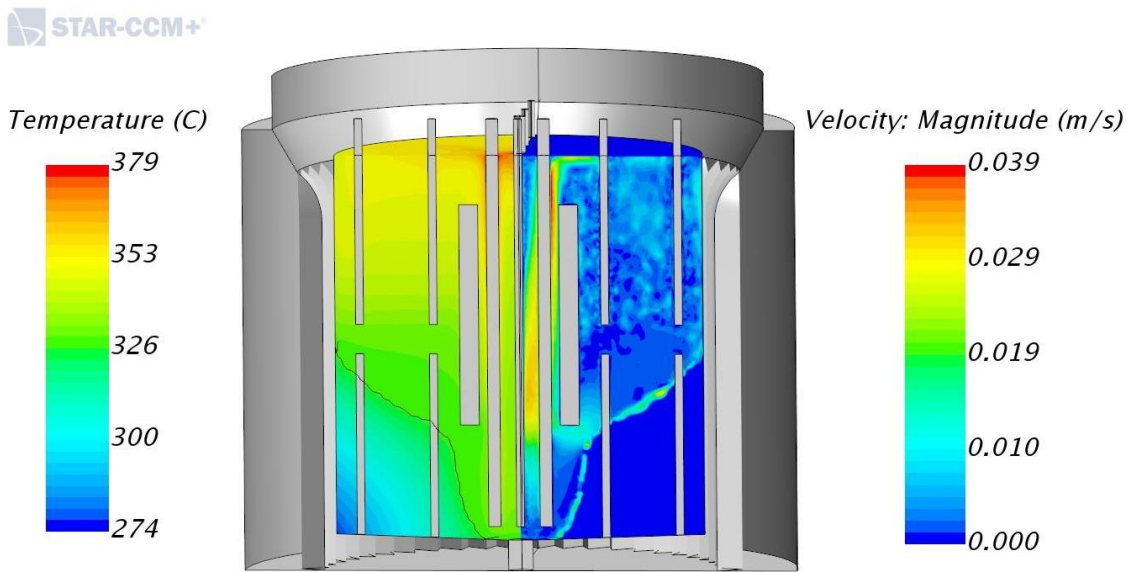


Fig. 10 Temperature and velocity fields at 33% of frozen Lead

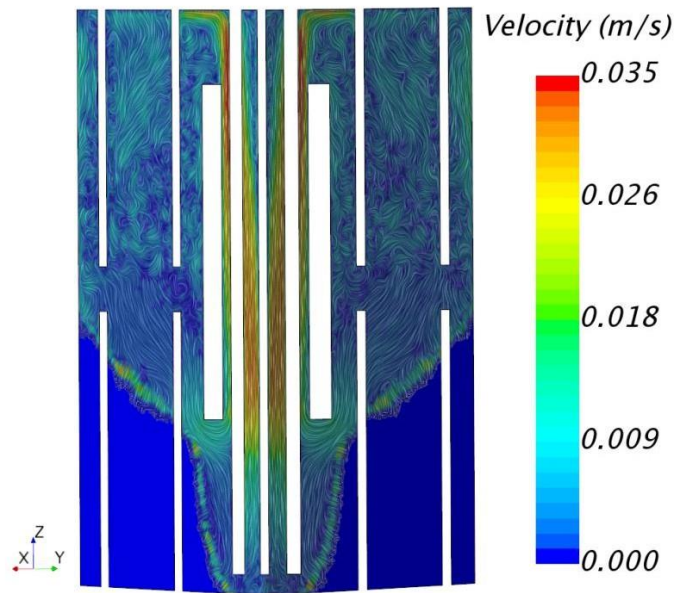


Fig. 11 Velocity vectors at 33% of frozen lead

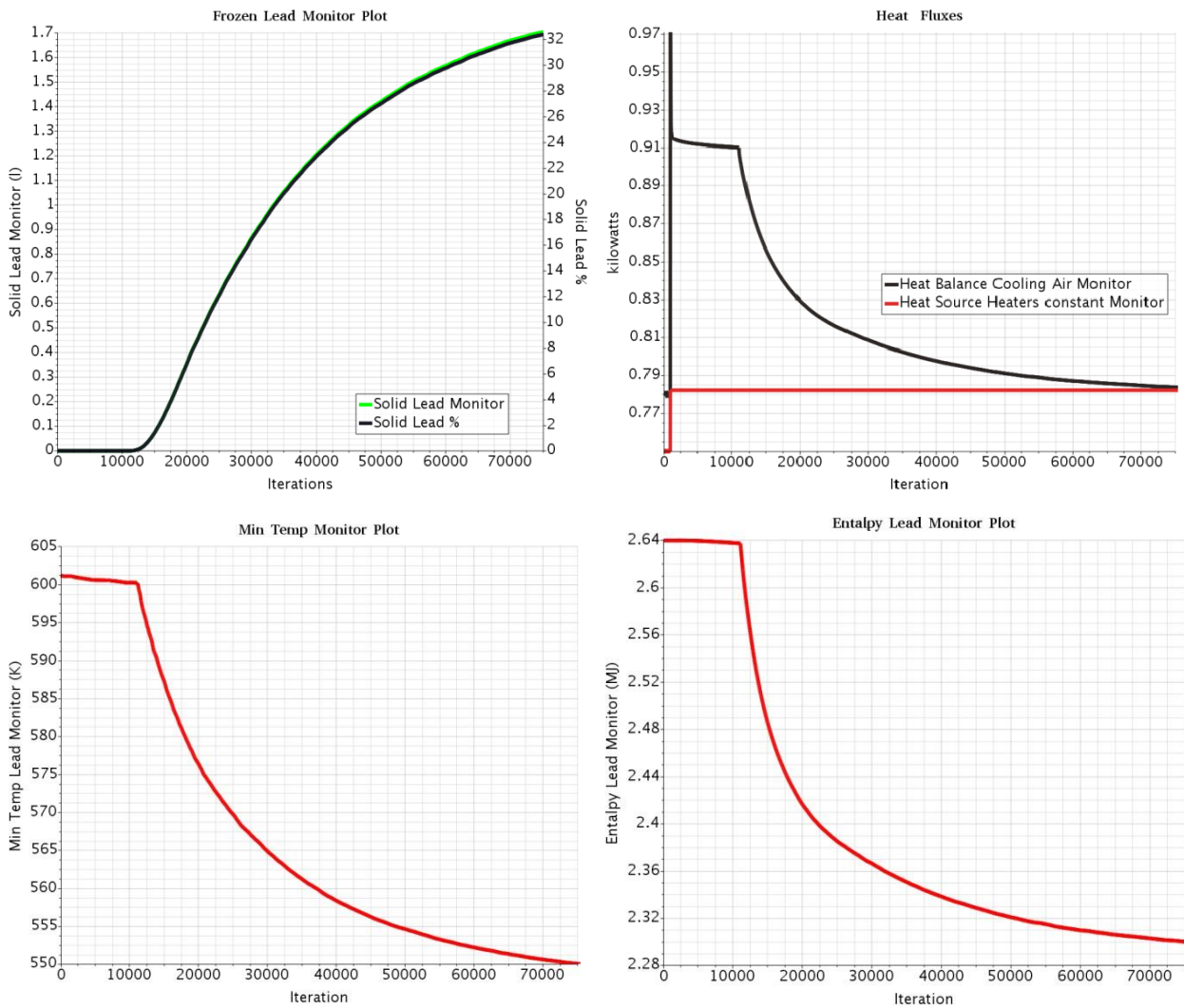


Fig. 12 Thermal trend in the case of 33% of frozen lead

The results from the steady state calculations in STAR-CCM+ are summarized in Table 3. The same results are compared with the CVR’s FLUENT results in Table 10.

Table 9: Results of steady-state simulations

Case	Air MFR [kg/s]	Heaters power [kW]	Solid fraction [%]	Max lead temp. [K]	Min lead temp. [K]	Max lead velocity [m/s]
1	0.146	3.12	0	695.9	601.1	0.0362
2	0.176	3.12	33	652.9	550.0	0.0398

Table 10: Comparative results of the steady state calculations

	Case 1		Case 2	
	FLUENT	STAR-CCM+	FLUENT	STAR-CCM+
Air Mass Flow Rate [kg/s]	0.145	0.146	0.176	0.178
Tmax [K]	695.27	695.90	651.65	652.90
Tmin [K]	606.40	601.10	547.05	550.06
Vmax Lead [m/s]	0.0373	0.0362	0.0392	0.0398
Frozen Fraction of lead [%]	0	0	42	33

4.2 Transient results

The transient calculation was started after reaching the convergence of the initial steady state. About 100 seconds of transient stabilization keeping the initial boundary condition was needed in order to obtain a stable transient calculation after it. The stabilization finished once the residuals are showing an ordinated and harmonic behaviour. The steps consisted in switching the steady state simulation just before the beginning of the solidification to unsteady state and initiate the solidification with a small time step (10^{-3} s), a large number of inner iterations (20) and with smaller under relaxation factors in the velocity and pressure solvers. Further on, the time step is progressively increased, until 0.1s, the inner iterations are diminished and the under relaxation factors are set to the initial default values.

For the simulation of the solidification, the air cooling boundary condition is switched to the maximum reachable from the blower: maximum cooling air velocity=6.25 m/s, MFR=0.5 kg/s, keeping the heat source constant.

This test was performed in order to evaluate how much time is needed to reach some specific fraction of frozen volume.

The same procedure was applied in the CVR’s model. The result of the transient simulation indicates that a frozen fraction of 33% (the maximum considered for the Phase 2 experimental run) is reached after 27 minutes in the STAR-CCM+ calculation and after 21 minutes in the FLUENT calculation.

An upper limit for the solidified volume was considered for the Phase 1 runs and was set to 67%. In the FLUENT model, this value is reached after 37 minutes while in STAR-CCM+ after 48 minutes. The curves of the solid volume fraction of lead, in liters and percentage, are shown in Fig. 13.

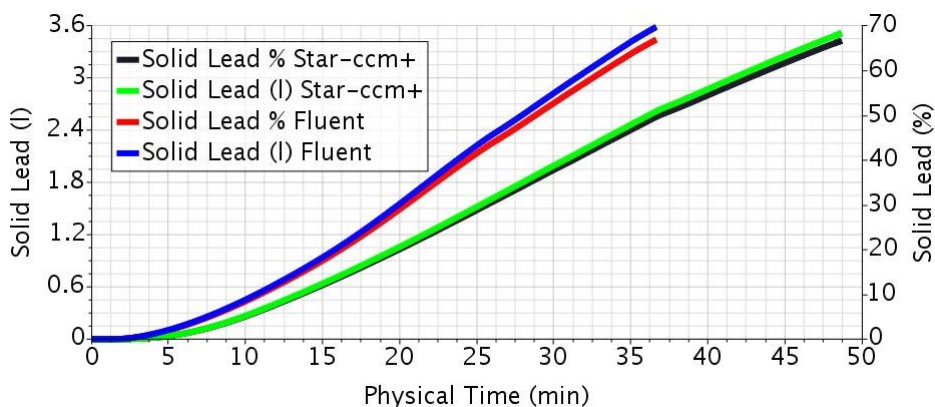


Fig. 13: Frozen fraction of lead in the two models

The trend of the solidification curve agrees with the curve of the heat flux removed by the cooling air which is slowly decreasing towards the thermal equilibrium and with the curve of the minimum temperature of the vessel and lead, as shown in Fig. 15.



Fig. 14 Trend of the heat fluxes

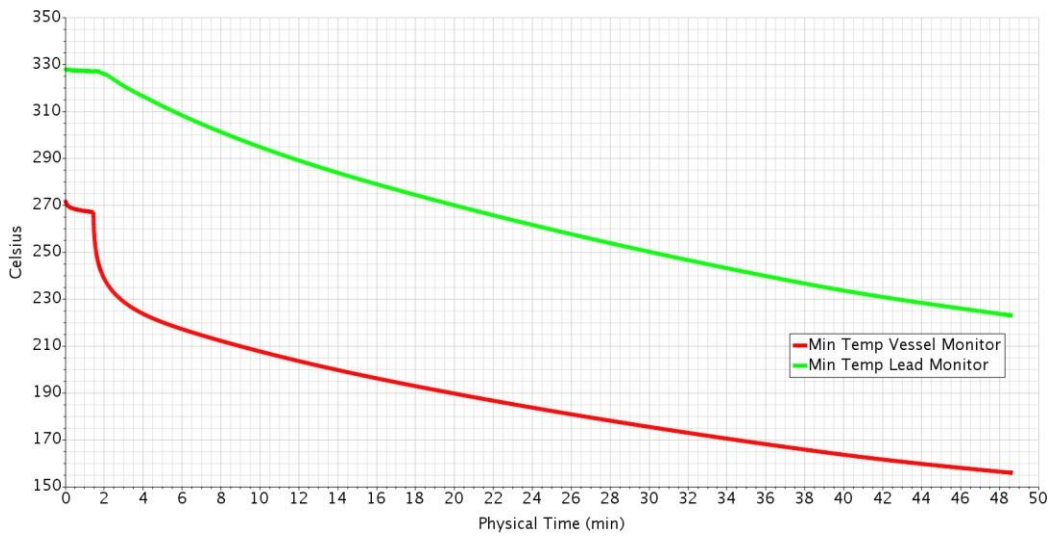


Fig. 15 Trend of the vessel and lead temperature

The temperature field, the velocity field and the iso-surface with the solidification front at 67% are shown in Fig. 16 and compared on the same scale with the similar fields obtained in Fluent.

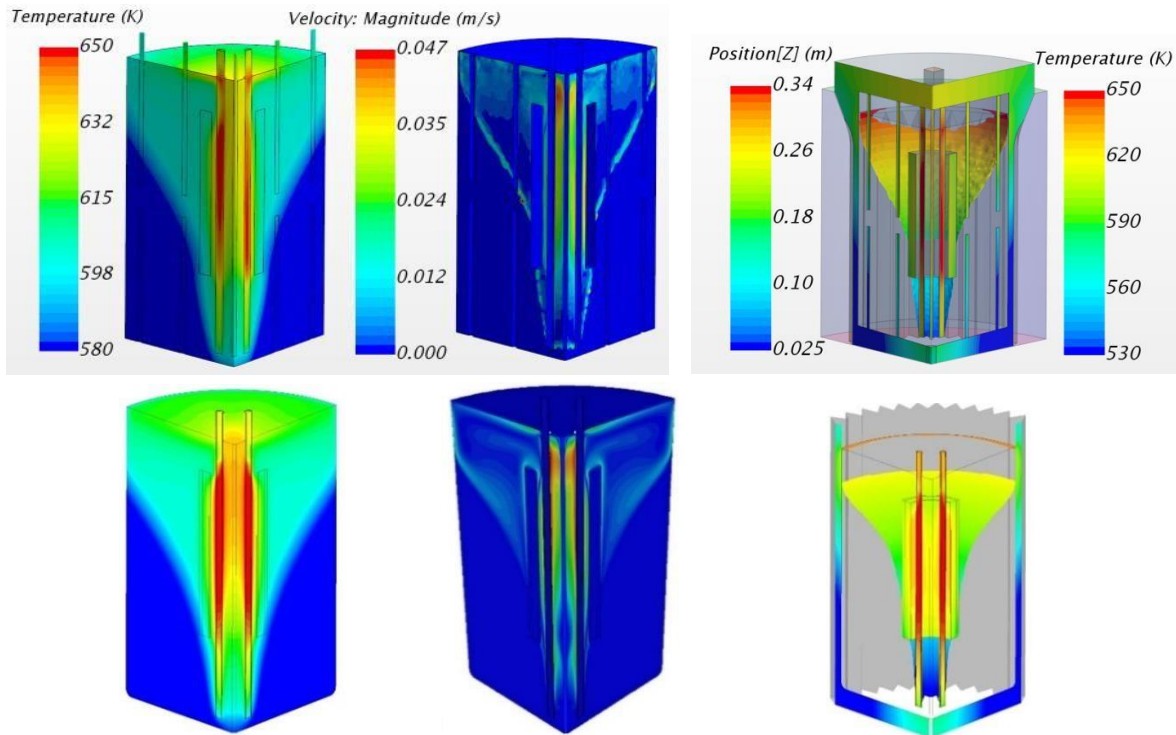


Fig. 16: Temperature and velocity fields and the iso-surface of the solidification front at 67% in the STAR-CCM+ model (top) and in the FLUENT model (bottom)

4.3 Technical issues about variable density flow in STAR-CCM+

Even if the simulation of the solidification was successively performed, particular attention was paid to the velocity field since at low values, below 0.02 m/s, the velocity field is clearly not resolved, as shown in the picture in Fig. 17 (left). The velocity is not updated both in the initial steady state phase and in steady and transient solidification phase.

In all the pre-test cases simulated in STAR-CCM+ and illustrated above, we agreed to fix the reference density to a value near the lead density, 10000 kg/m³ and we focused the attention on the simulation of the solidification. Getting close to the post-test phase, we concentrated our attention also on the analysis of the velocity field.

In order to find the correct configuration of the velocity field, we tested various values of the reference density on a simplified geometry, without the cooling air channel and without the solid vessel. The temperature at the walls of the lead domain was imposed first to 605 K, then to 601 K and also to 550 K to see the solidification. A constant heat source was defined in the heater. We obtained that the velocity field is correctly resolved if the reference density is set to the effective value of the lead density (Fig. 17-right). With a density slightly smaller, like 10000 kg/m³, as it was used in the Sesame-Stand simulations, the velocity is not correctly updated, as shown in the picture in Fig. 17 (centre).

For a temperature at the wall of 605 K, the lead density is 10.667 kg/m³. For a temperature of 601 K, the lead density is 10672 kg/m³. The velocity fields obtained in this case quickly reaches the expected correct configuration. In the picture in Fig. 17 (right), the velocity vectors are illustrated in the case of the temperature at 601 K and the reference density fixed at 10672 kg/m³ and are compared with the unresolved velocity vector fields.

These tests performed on the simplified geometry indicate that the dependence of the solution on the reference density is an important issue that will be carefully taken into consideration in the post-test simulations. An interaction with the STAR-CCM+ developers will also be activated.



Fig. 17 Velocity vectors in SESAME –stand configuration (left) compared with the same configuration in a simplified geometry (center) and with the correct configuration of velocity field in simplified geometry (right)

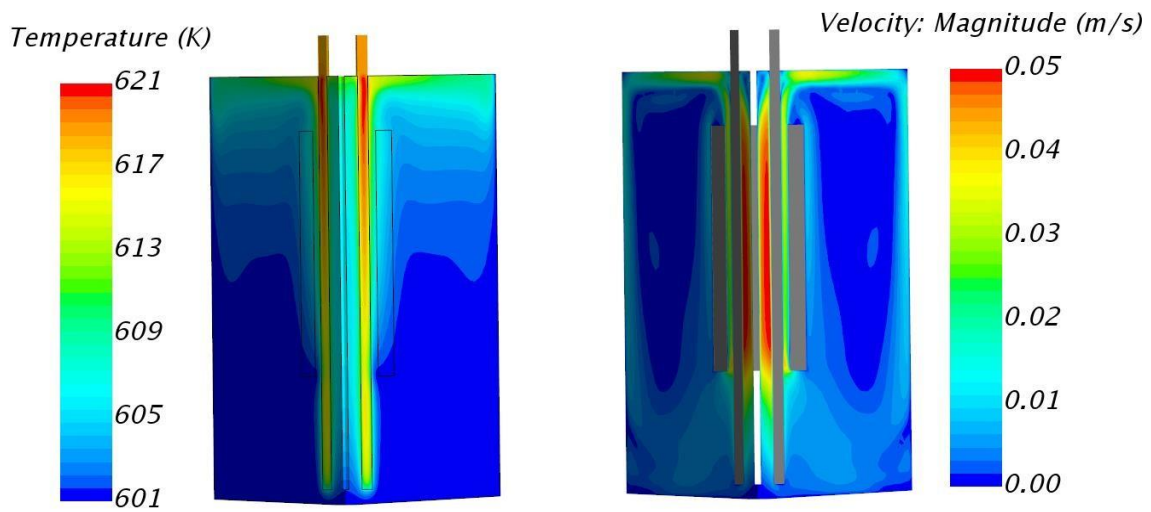


Fig. 18 Temperature and velocity fields in correct configuration

5. CONCLUSIONS

An articulated computational model of the SESAME–Stand experimental facility was built in close collaboration with CVR with useful exchange of information about geometry, but also numerical approach and results comparison.

The model has been progressively improved thanks to this collaboration and the construction of the numerical model has taken only progressively all the features of the real experimental setting.

The model able to simulate the behavior in case of solidification of the liquid lead inside the SESAME-stand facility was developed using STAR-CCM+ while the CVR’s model was developed using Fluent. An agreed procedure to reach convergence in every working condition was defined between the two simulation codes.

Technical/numerical issues have been partially overcome: the initial phase of the freezing in steady state could be realized only by means of an intermediate phase with transient settings. The velocity field is correctly obtained on a simplified version of the geometry only if the reference density in the lead continuum is set to the effective density of the lead fixed at the external walls. In the case with the complete geometry, the correct velocity configuration was not yet obtained. Moreover, the dependence of the solution on the reference density during the solidification remains an important issue to be resolved in the post-test phase.

Possible initial and final steady state conditions for the experimental runs were found according to the technical needs. For the fixed heat source of 3.12 kW, steady state freezing in the range 0-33% is obtained for cooling air velocity in the range 1.8-2.2 m/s.

Comparison with the Fluent model shows similar results in steady state and differences in the transient calculation.

A first transient simulation was successfully performed. Fast freezing of 33% and 67% from onset is obtained respectively in 27 minutes and 48 minutes showing a quite linear trend. The same percentage of frozen lead is reached faster in the CVR's model (21 and respectively 37 minutes).

The differences might be caused by different approaches in the geometry simplifications, mesh or by numerical uncertainties. The suitability of the codes will be evaluated in the following stage of the SESAME project, once the collection of experimental data is completed. Moreover, it seems quite important to carefully measure the air heating from the outlet air temperature and mass flow rate.

References

- [1] STAR-CCM+ User's Guide Release 12, Siemens PLM Software, 2017
- [2] I. Dofek, O. Frybort, J. Vit, M. Sinc, "Description of the Meliloo – stand test facility and test matrix", SESAME project deliverable, 2016.
- [3] M. Iannone, I. Dofek, T. Melichar, W. Borreani, G. Lomonaco, V. Moreau, M. Profir, Development of CFD models and pre-test calculations for thermal-hydraulics and freezing experiments on Lead coolant, Proceedings of the *International Conference Nuclear Energy for New Europe*, Bled, Slovenia, September 11-14, 2017
- [4] B. Niceno, A. Badillo: "Summary for the recommended physical properties for the main fluid and liquid materials used for the MELILOO-stand and TALL-3D freezing experiments." SESAME project deliverable, 2017.